Appendix O
Socket Calculations

1.0 Introduction

The cables supporting the telescope were connected to the platform, towers, and anchors through zinc-filled spelter sockets. The telescope collapsed after three sockets failed at the top of Tower 4 (Appendix E), and significant cable slip was observed on other sockets before the collapse (Appendix D). After the collapse, six sockets were recovered from the site and tested to determine dimensions, material properties and wire broom geometry (Appendix M). One socket was also load-tested to failure (Appendix O).

To analyze how the socket properties may have caused or contributed to the observed cable slips and socket failures, we developed a mathematical model for the strength of zinc-filled spelter sockets. The model and its application to the telescope's sockets are presented in this appendix.

In a zinc-filled spelter socket, forces are transferred through a composite medium where a zinc continuum fills the gaps between discrete steel wires. This material has complex mechanical properties, and engineering assumptions were made to simplify the mathematical model. The model is not intended to predict any specific cable slip distance or socket failure load, but to analyze how a socket's property affects its mechanical behavior and strength.

In this appendix, the failure of a cable near a socket is referred to as a *socket failure* as long as multiple wires fractured inside the socket. The *cable slip* is the distance by which a cable moved longitudinally with respect to the socket before failure. The *socket casting* is the composite medium that includes the cast zinc and the enclosed steel wires.

2.0 Model Basis

The proposed model was developed to replicate the behavior of the telescope's sockets that failed or exhibited the most significant cable slips. These sockets are referred to as the *damaged sockets* in the following.

2.1 Observations

As shown in Figure 5 through Figure 1, three key features were observed on the damaged sockets: a displaced inner core, some ruptured outer wires, and/or some slipped outer wires.

Socket **M4N_T** (Figure 1) was the first socket to fail, on August 10, 2020. In this case, an inner core of the casting slipped out of the socket entirely, and multiple outer wires ruptured. The socket and slipped-out core and cable end were analyzed by Wiss, Janney, Elstner Associates (WJE) and the NASA Engineering and Safety Center (NESC), and their findings were provided in a report[1]. Among these findings, it was observed that some wire located outside the core had slipped with respect to the cast zinc.

[1] Wiss, Janney, Elstner Associates (WJE). *Auxiliary Main Cable Socket Failure Investigation.* June 21, 2021. Draft report provided by WJE.

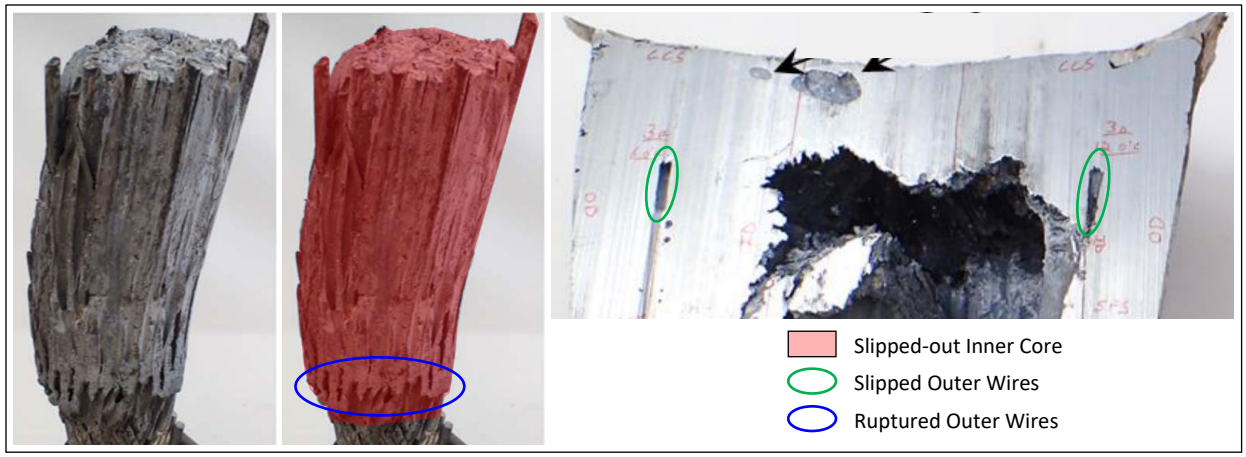

Figure 1: Slipped-out inner core, and ruptured and slipped outer wires in socket M4N_T
(photos: WJE[2]).

Socket **M4-4_T** (Figure 2) failed on November 6, 2020, approximately three months after the first socket failure (M4N_T). The first socket failure had caused four outer wires to rupture in M4-4_T. The socket's casting was cut open after the collapse, and on the cut surface we observe the significant displacement of an inner core.

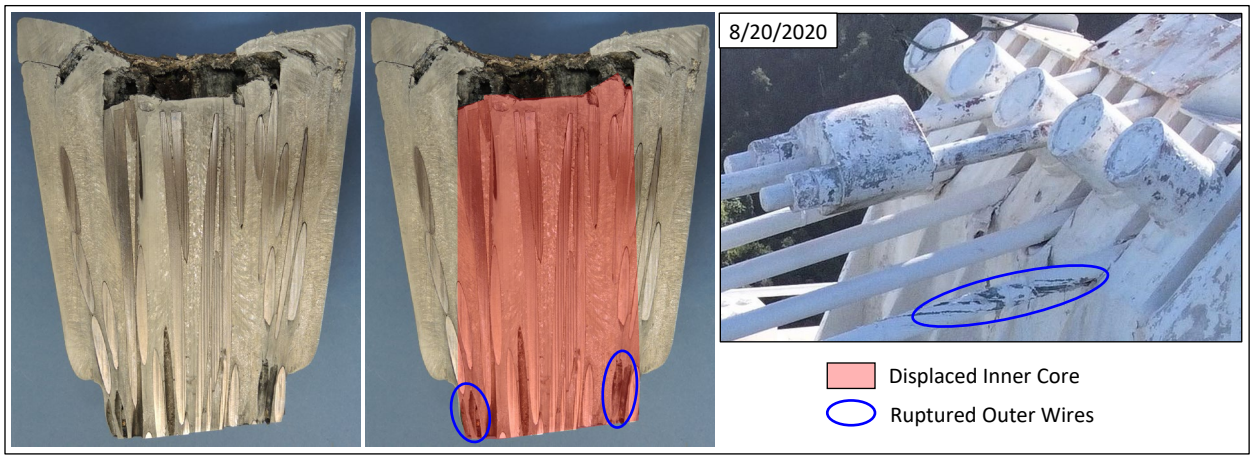

Figure 2: Displaced inner core and ruptured outer wires in socket M4-4_T
(left and center photos: Socotec, right photo: NAIC Arecibo Observatory, a facility of the NSF).

Socket **M4-2_T** (Figure 3) failed on December 1, 2020, which triggered the collapse of the telescope. At least seven outer wires had ruptured before the socket's failure: one wire ruptured after the first socket failed (M4N_T), another wire ruptured when the second socket failed (M4-4_T), and at least five additional wires ruptured in the three weeks preceding the collapse. Photographs of the back of the socket taken before and after the collapse show that an inner core of the socket's casting displaced before and possibly during the socket failure.

[2] Wiss, Janney, Elstner Associates (WJE). *Auxiliary Main Cable Socket Failure Investigation.* June 21, 2021. Draft report provided by WJE.

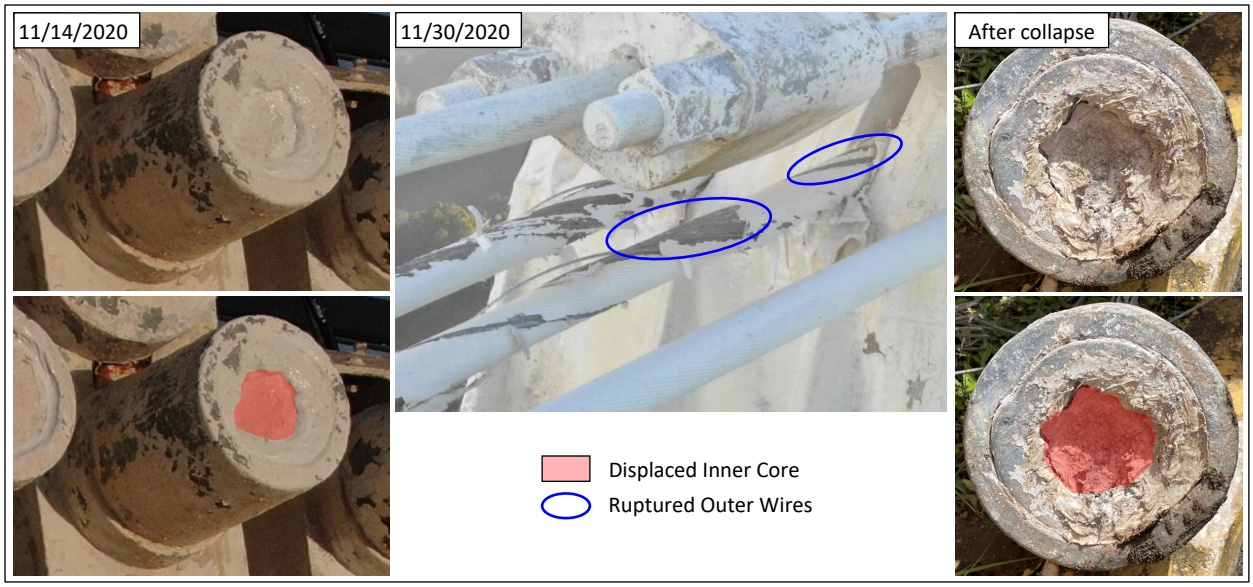

Figure 3: Displaced inner core and ruptured outer wires in socket M4-2_T
before failure (left and center) and after failure (right)
(left and center photos: NAIC Arecibo Observatory, a facility of the NSF).

Socket **B12W_G** (Figure 4) exhibited the largest cable slip among the telescope's sockets before the collapse. The casting was cut open after the collapse, and on the cut surface we observe that an inner core has displaced within the casting, with cracks opening at the back of the core. We also observe that the wire ends located outside of the core have slipped with respect to the cast zinc. A one-inch-thick slice of the casting was radiographed with neutron imaging, and the radiograph reveals that every wire end located outside of the core has slipped.

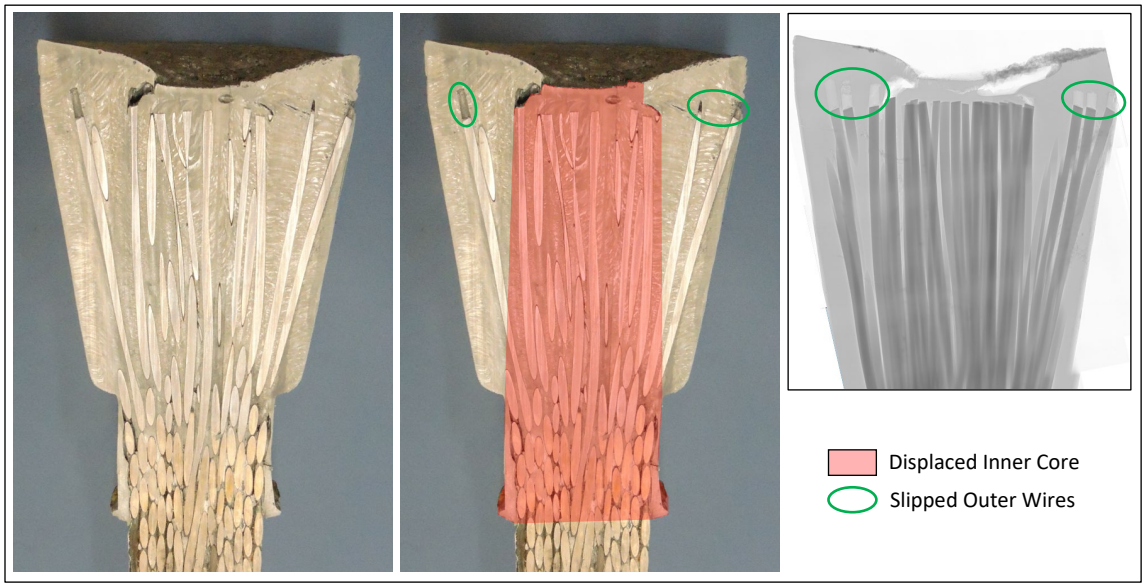

Figure 4: Displaced inner core and slipped outer wires in socket B12W_G
(left and center photos: Socotec; right photo: Adrian Brügger, Columbia University - Oak Ridge National Laboratory).

Socket **B4S_G** (Figure 5) did not fail before or during the telescope's collapse, but was recovered from the site and load-tested to failure as part of the investigation (Appendix O). The load test was ended after seven outer wires ruptured inside the socket. When the seventh wire ruptured, the cable tension was two percent higher than the

cable's Minimum Breaking Strength. The socket's casting was cut open after the test. On the cut surface, we observe that an inner core has displaced within the casting, with cracks opening at the back of the core. The seven ruptured wires are outer wires that used to extend across the core surface towards the socket wall.

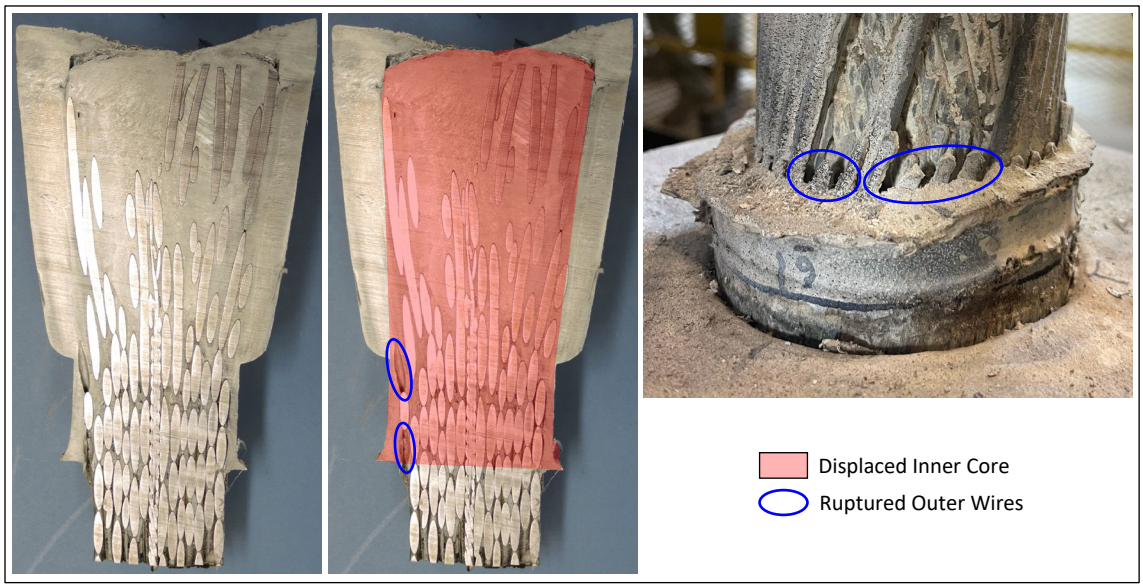

Figure 5: Displaced inner core slip and ruptured outer wire in socket B4S_G after tensile test to failure
(left and center photos: Socotec).

Significant permanent deformation occurred within the zinc casting of the damaged sockets. As shown in Figure 6, the deformation is visible near the surface of the displaced core in some of the castings investigated. This indicates that at least some of the core displacement occurred through plastic deformation and/or creep of the zinc, which we refer to as zinc *flow*.

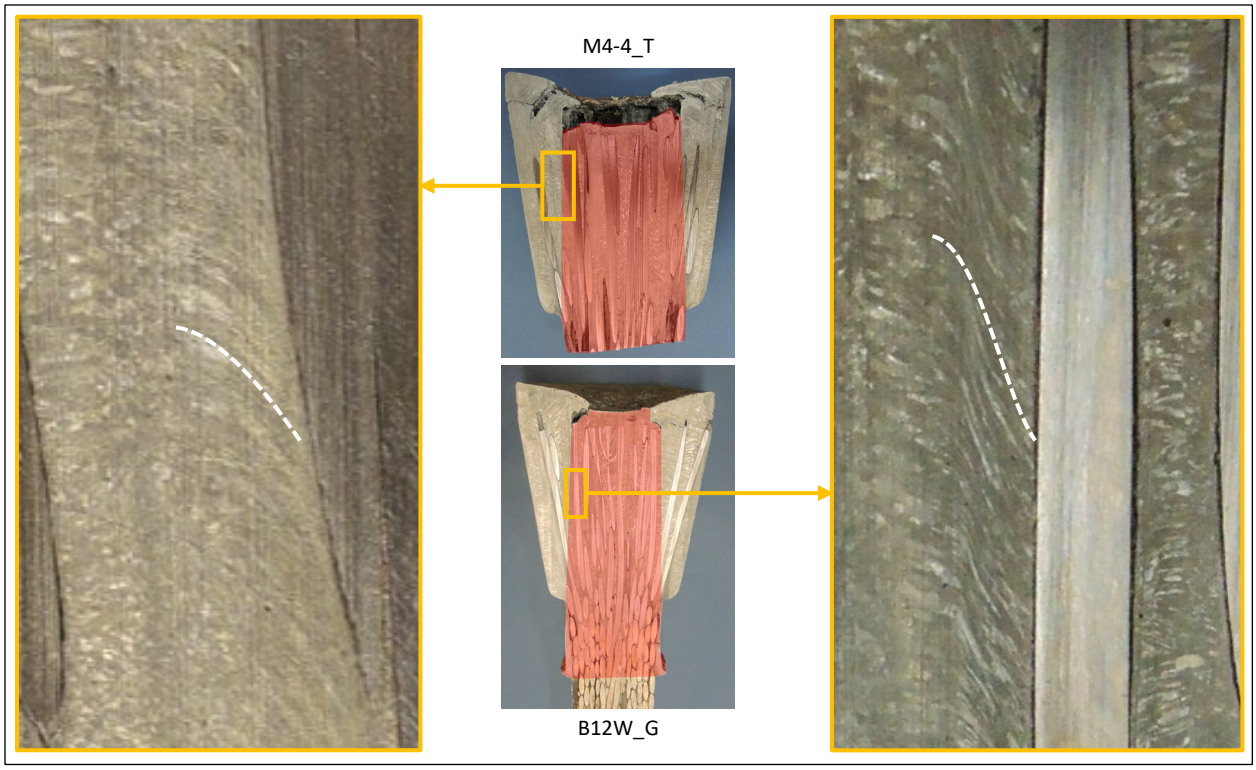

Figure 6: Zinc flow near surface of slipped core in sockets M4-4_T and B12W_G *(photos: Socotec).*

2.2 Idealization

The zinc casting is the interface that transfers the cable tension to the socket. As shown in Figure 7, the casting is held inside the socket by a combination of compression and shear on the casting surface, and bearing on the socket's shoulder if the socket has one.

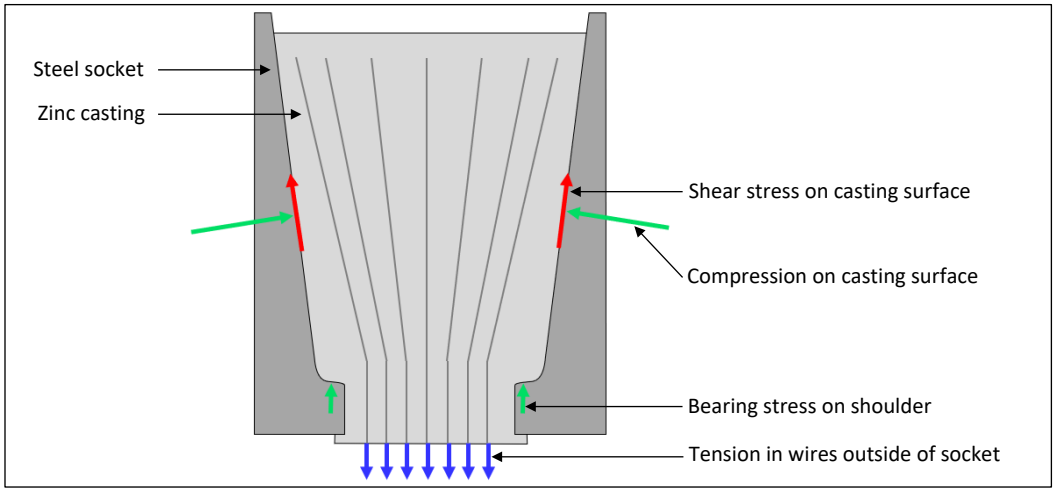

Figure 7: Zinc casting equilibrium.

In each of the fives damaged sockets considered above, the displacement of an inner core was observed within the socket's casting. We therefore propose to analyze the strength of zinc-filled spelter sockets with a model that distinguishes the core from the rest of the casting. As shown in Figure 8, the *core* is idealized as a cylinder aligned

with the cable direction and extending over the entire casting length. The casting outside the core is called the *perimeter*, and any wire that passes through the core surface is called a *crossing wire*. Figure 8 also shows the forces acting on the core. The cable tension tends to pull the core out of the socket, and the core is held in place by a combination of tension in the crossing wires and shear stress on the core surface. There is also a radial compressive stress field in the socket, which allows to develop friction on the core surface and between the wires and the zinc.

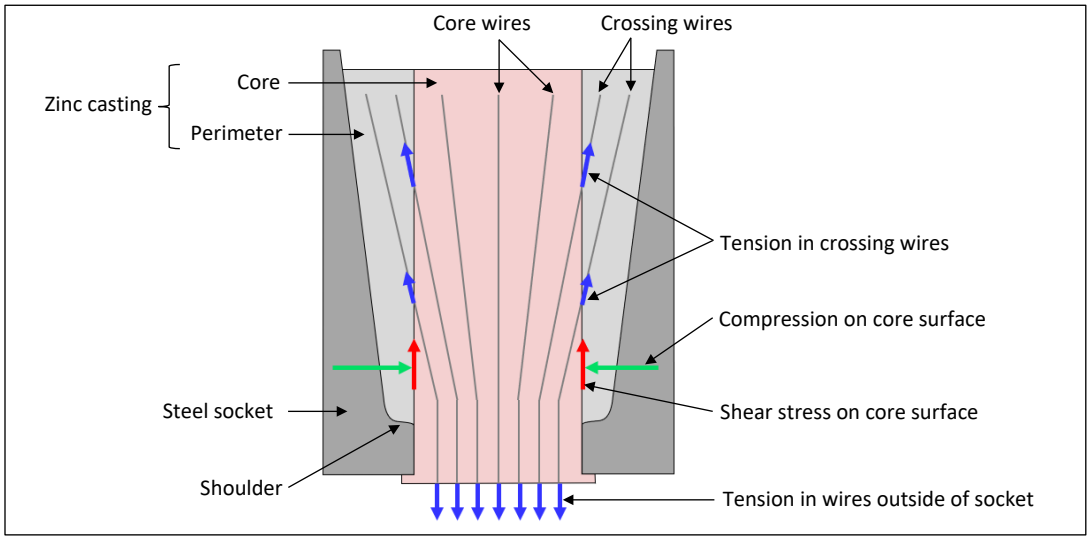

Figure 8: Casting core equilibrium and model nomenclature.

3.0 Model Formulation

A set of equations was derived to calculate the maximum force that can be transferred out of the core through tension in the crossing wires and shear on the core surface. The tension and shear load transfer mechanisms are considered separately in this section. Whether they can occur simultaneously is discussed in further sections, when applying the model to the telescope's sockets.

3.1 Applicability to Sockets with and without Shoulder

A spelter socket may or may not have a shoulder, which is a step in the diameter of the socket's cavity. All of the damaged sockets considered above have a shoulder, but some other sockets of the telescope, such as the platform-end sockets of the auxiliary main cables, do not have the shoulder. Spelter sockets with and without shoulder are also found in other existing structures. Our finite element analysis results (Appendix P) indicate that the presence of a shoulder does not affect the long-term behavior of the socket casting. Therefore, for those sockets that include a shoulder, our model consider a simplified casting geometry where the shoulder is bypassed (Figure 9). With this simplification, the proposed model is applicable to zinc-filled spelter sockets with and without shoulders.

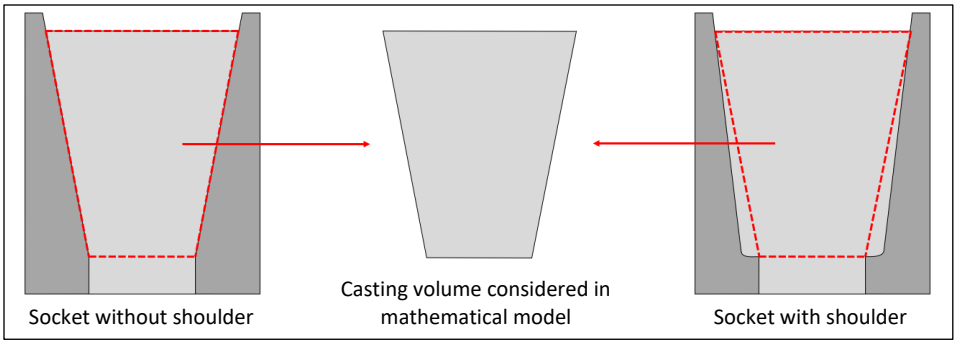

Figure 9: Casting volume considered in socket strength model.

3.2 Pressure on Casting Surface

The normal and tangential pressures acting on the casting surface are determined from the equilibrium of the entire casting (Figure 10).

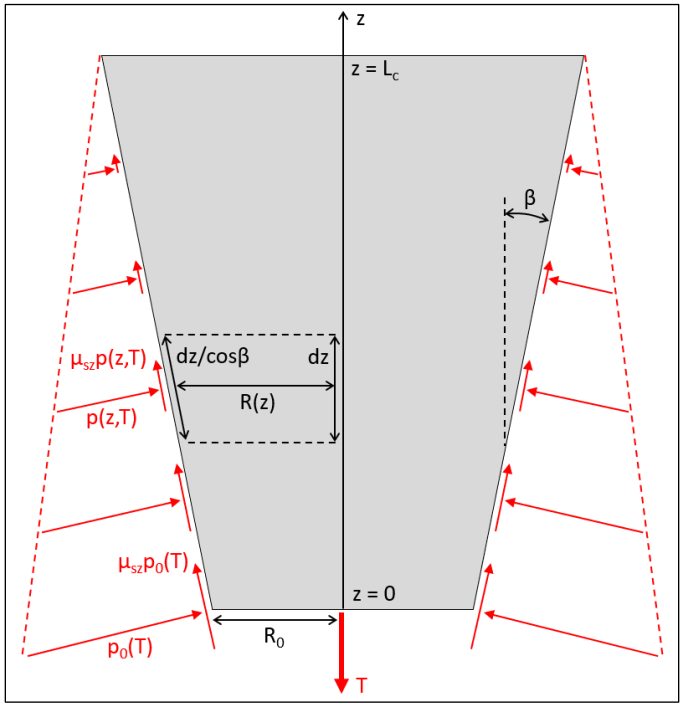

Figure 10: Zinc casting equilibrium under cable tension and stresses on casting surface.

The shape of the casting is defined by three dimensions: smaller diameter R_0, length L_c, and slope β. The variable *z* designates a position along the socket axis, and any quantity that varies with z is noted as such in the calculations (e.g. *R(z)*). The radius of the casting varies along the axis:

$$R(z) = R_0 + z\,tan\beta \quad [1]$$

The cable tension is noted *T*. The cable tension is a key parameter in the analysis of the socket failures, and any quantity that depends on the cable tension is noted as such in the calculations (e.g. $p_0(T)$). The normal pressure on

the casting surface, noted *p(z,T)*, is assumed to vary linearly along the socket axis, consistently with published experimental results.[3] With $p_0(T)$ its maximum value, the normal pressure distribution is as follows:

$$p(z,T) = p_0(T)\left(1 - \frac{z}{L_c}\right) \quad [2]$$

The friction coefficient between the steel socket and zinc casting is noted μ_{sz}. The cable tension is in equilibrium with the normal and tangential stresses on the casting surface:

$$T = \int_{z=0}^{L_c} (p(z,T)sin\beta + \mu_{sz}p(z,T)cos\beta)2\pi R(z)\frac{dz}{cos\beta}$$

Replacing with [1] and [2] in the equation above, and integrating along the casting's length:

$$T = 2\pi p_0(T)(tan\beta + \mu_{sz}) \int_{z=0}^{L_c} \left(1 - \frac{z}{L_c}\right)(R_0 + z\, tan\beta)dz$$

$$T = \pi p_0(T)(tan\beta + \mu_{sz})L_c\left(R_0 + \frac{tan\beta}{3}L_c\right)$$

The maximum pressure on the casting surface, which occurs at the front end of the socket, is therefore:

$$p_0(T) = \frac{3T}{\pi L_c(3R_0 + L_c tan\beta)(tan\beta + \mu_{sz})} \quad [3]$$

[3] Klaus Freyer. *Drahsteile*. Springer Vieweg Berlin. 1994.

3.3 Shear Capacity on Core Surface

In the castings of the damaged sockets, we observed that a central core had slipped with respect to the rest of the casting (section 2.0 above). The core is highlighted in Figure 11 and Figure 12, and its radius is considered as a variable noted *r*. Any quantity that depends on the core radius is noted as such in the calculations (e.g. $S_c(r)$).

In the following, we determine the maximum shear force that can be developed on the core surface to resist the cable pull. The maximum shear force is developed through zinc cohesion (Figure 11) and zinc-to-zinc friction (Figure 12).

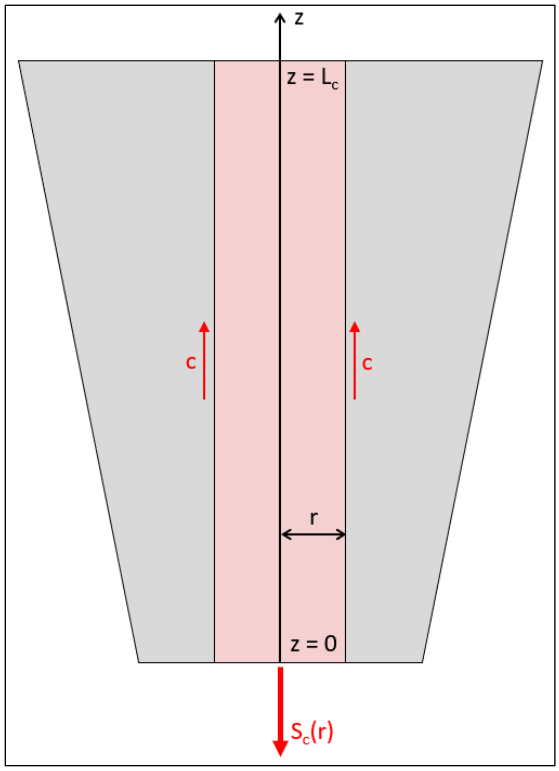

Figure 11: Core cohesion capacity.

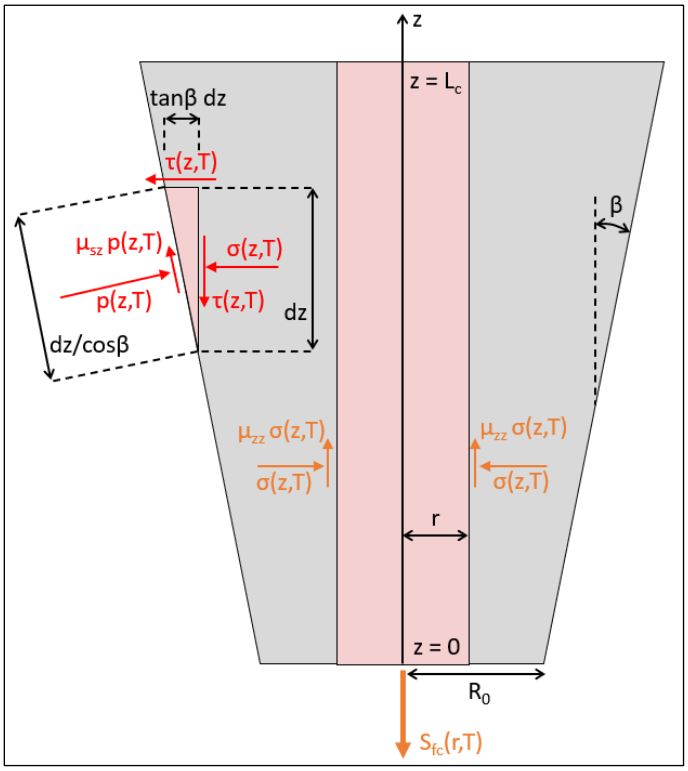

Figure 12: Core confinement friction capacity.

The maximum force that can be resisted through zinc cohesion on the core surface is called the *cohesion capacity* and noted $S_c(r)$. The cohesion capacity is the resultant of the zinc's cohesion stress *c* applied to the surface area of the core (Figure 11):

$$S_c(r) = 2\pi r L_c c \qquad [4]$$

As shown in Figure 12, the normal and tangential pressures on the casting surface induce a radial stress $\sigma(z,T)$ and a shear stress $\tau(z,T)$ in the casting volume. The equilibrium of an infinitesimal zinc volume near the casting surface is as follows:

$$\sigma(z,T)dz + \tau(z,T)tan\beta\, dz = p(z,T)(cos\beta - \mu_{sz}sin\beta)\frac{dz}{cos\beta}$$

$$\tau(z,T)dz = p(z,T)(sin\beta + \mu_{sz}cos\beta)\frac{dz}{cos\beta}$$

The above system can be solved to determine the radial and shear stresses in the casting:

$$\sigma(z,T) = p(z,T)(1 - 2\mu_{sz}tan\beta - tan^2\beta) \quad [5]$$

$$\tau(z,T) = p(z,T)(tan\beta + \mu_{sz})$$

The radial stress in the casting is compressive and acts as a confinement stress on the core, allowing to develop friction on the core surface. This friction is zinc-to-zinc, and the corresponding friction coefficient is noted μ_{zz}. The maximum force that can be resisted by this friction is called the *confinement friction capacity* and noted $S_{fc}(r,T)$. From the equilibrium of the core shown in Figure 12, the confinement friction capacity is as follows:

$$S_{fc}(r,T) = \int_{z=0}^{L_c} \mu_{zz}\sigma(z,T)\, 2\pi r dz$$

Replacing with [2] and [5] in the equation above, and integrating along the casting's length:

$$S_{fc}(r,T) = 2\pi r\mu_{zz}p_0(T)(1 - 2\mu_{sz}tan\beta - tan^2\beta) \int_{z=0}^{L_c} \left(1 - \frac{z}{L_c}\right) dz$$

$$S_{fc}(r,T) = \pi r\mu_{zz}L_c p_0(T)\,(1 - 2\mu_{sz}tan\beta - tan^2\beta) \quad [6]$$

3.4 Crossing Wires Capacity

A crossing wire is a wire that crosses through the surface of the core, as shown in Figure 13. Whether a wire is a crossing wire depends on the wire's geometry and the core's radius. The set of crossing wires for a given core radius *r* is note *I(r)*. The geometry of each crossing wire is described by two parameters that depend on the core radius: the position $z_i(r)$ of the crossing point along the socket axis, and the angle $\gamma_i(r)$ between the wire and socket axis at the crossing point. The length of wire inserted in the casting is assumed equal for all wires and noted L_w.

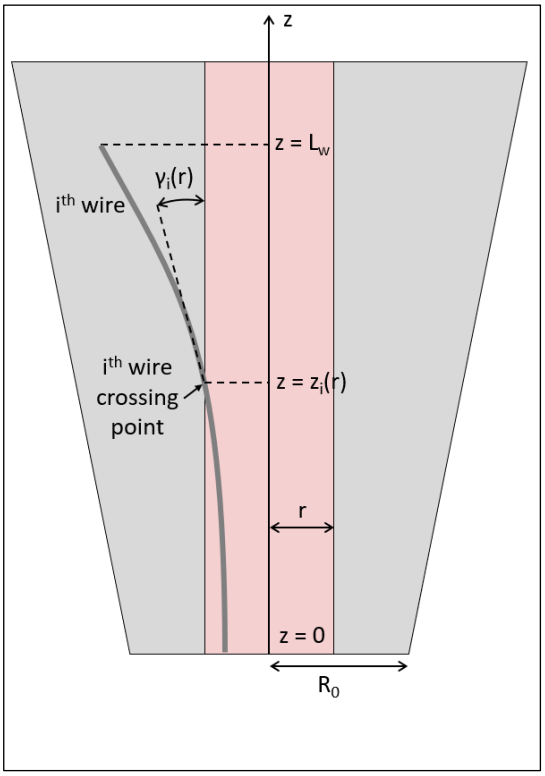

Figure 13: Crossing wire geometry.

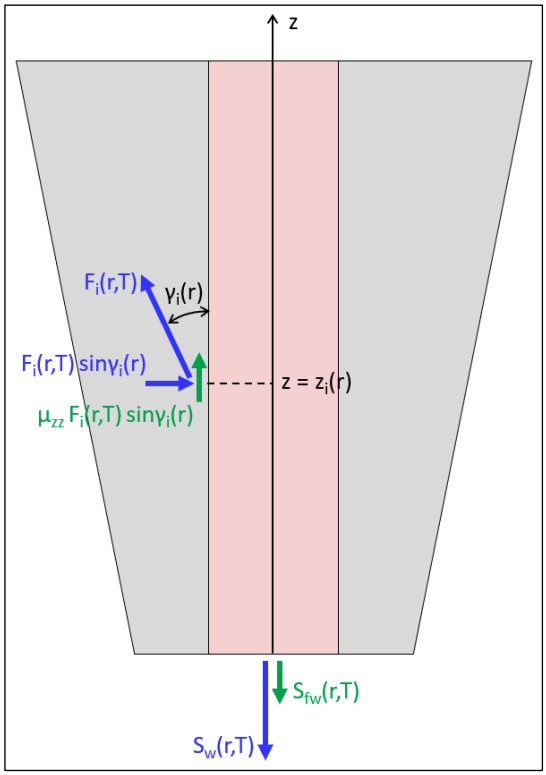

Figure 14: Crossing wire capacity

The maximum tension that a crossing wire can develop at the crossing point is noted $F_i(r,T)$. The longitudinal component of the crossing wire tension directly resists core pull-out, and the sum of this component over all crossing wires is called the *crossing wires capacity* and noted $S_w(r,T)$.

$$S_w(r,T) = \sum_{i \in I(r)} F_i(r,T) cos\gamma_i(r) \quad [7]$$

The radial component of the crossing wire tension induces an additional radial compressive stress on the core surface, which allows to develop additional friction on the core surface (Figure 14). The maximum force that can be resisted by this friction is called the *crossing wires friction capacity* and noted $S_{fw}(r,T)$.

$$S_{fw}(r,T) = \mu_{zz} \sum_{i \in I(r)} F_i(r,T)\ sin\gamma_i(r) \quad [8]$$

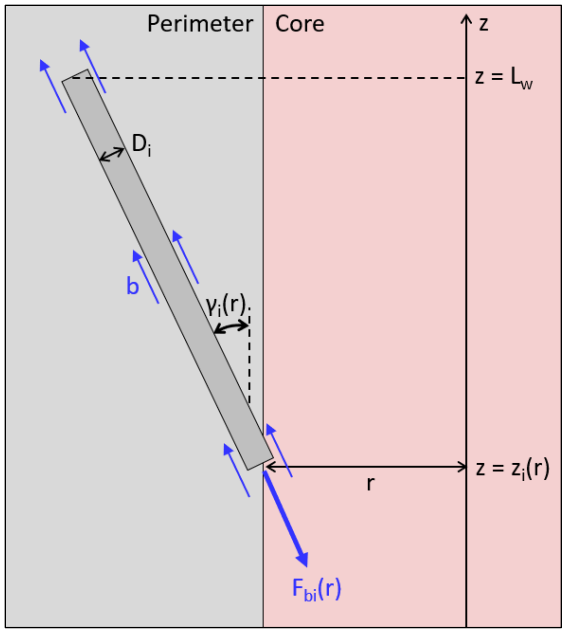

Figure 15: Wire slip resistance from bond with zinc.

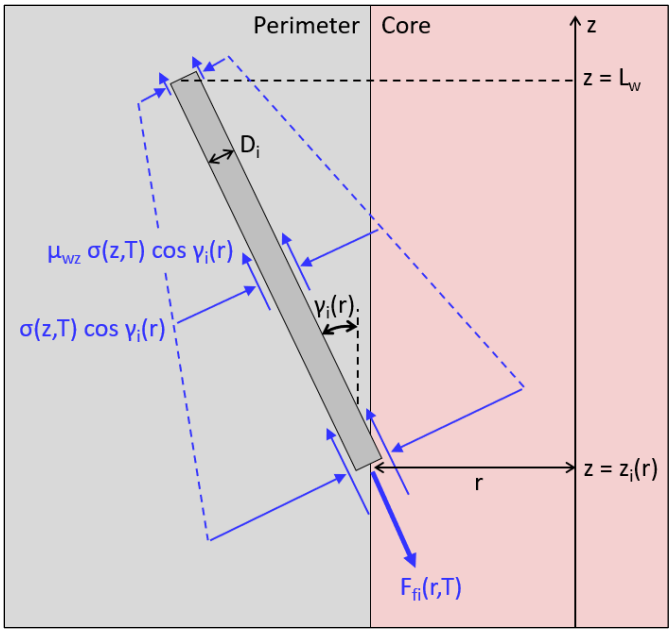

Figure 16: Wire slip resistance from friction with zinc.

The tensile behavior of the wires is assumed elastic-perfectly plastic. The maximum tension that a wire can develop before yielding and eventually rupturing is called the *nominal wire strength* and noted F_{ui}. With D_i the wire diameter and u a nominal critical stress, the nominal wire strength is as follows:

$$F_{ui} = \frac{\pi {D_i}^2 u}{4} \quad [9]$$

The end of each crossing wire is embedded in the perimeter zinc (zinc volume outside of core). As the core pulls out, the wire ends can slip in the perimeter zinc if the slip resistance is not sufficient. Wire slip is resisted by bonding and friction with the perimeter zinc.

A crossing wire's *bond capacity* $F_{bi}(r)$ is the maximum wire tension that can be resisted by the mechanical bond between the wire and perimeter zinc. With b the maximum bond stress in shear, the wire's bond capacity is as follows (Figure 15):

$$F_{bi}(r) = \pi D_i b \frac{L_w - z_i(r)}{cos\gamma_i(r)} \quad [10]$$

A crossing wire's *friction capacity* $F_{fi}(r,T)$ is the maximum wire tension that can be resisted in friction between the wire and perimeter zinc. This friction is developed based upon the radial compressive stress $\sigma(z,T)$ present in the casting and the friction coefficient μ_{wz} between wire and zinc. The wire's friction capacity is as follows (Figure 16):

$$F_{fi}(r,T) = \int_{z=z_i(r)}^{L_w} \mu_{wz}\sigma(z,T)cos\gamma_i(r)\pi D_i \frac{dz}{cos\gamma_i(r)}$$

Replacing with [2] and [5] in the equation above, and integrating along the wire length in the perimeter zinc:

$$F_{fi}(r,T) = \mu_{wz}\pi D_i(1 - 2\mu_{sz}tan\beta - tan^2\beta)p_0(T) \int_{z=z_i(r)}^{L_w} \left(1 - \frac{z}{L_c}\right) dz$$

$$F_{fi}(r,T) = \mu_{wz}\pi D_i p_0(T)(1 - 2\mu_{sz}tan\beta - tan^2\beta)\left(L_w - z_i(r)\right)\left(1 - \frac{L_w + z_i(r)}{2L_c}\right) \quad [11]$$

The maximum tension $F_i(r,T)$ that a crossing wire can develop to resist core pull-out is the least of either the wire's nominal strength or the sum of the wire's bond and friction capacities:

$$F_i(r,\ T) = min\ \left(F_{ui}(r),\ F_{bi}(r) + F_{fi}(r,T)\right) \quad [12]$$

A crossing wire is described as *fully developed* if it ruptures before slipping:

$$F_{bi}(r) + F_{fi}(r,T) > F_{ui}(r)$$

Conversely, a crossing wire is described as *partially developed* if it slips before rupturing:

$$F_{bi}(r)\ + F_{fi}(r,T) < F_{ui}(r)$$

3.5 Total Core Capacity

The *total core capacity* $S_t(r,T)$ is the maximum force that can be developed in the casting to resist core pull-out, considering shear on the core surface and tension in the crossing wires:

$$S_t(r,T) = S_c(r) + S_{fc}(r,T\ ) + S_w(r,T) + S_{fw}(r,T) \quad [13]$$

The total core capacity depends on the cable tension T because the friction components of the capacity depend on the radial compressive stress produced by squeezing casting into the cone-shaped socket under the cable tension.

When considering a core of smaller diameter than the cable, only part of the cable tension T is pulling on the core. This *core tension* is noted $S(r,T)$ and calculated based on the total wire area in the core section $A_S(r)$ and the total wire area in the cable section A_T:

$$S(r,T) = \frac{A_S(r)}{A_T}T \quad [14]$$

For a given core diameter, the *cable pullout tension* $T_p(r)$ is the cable tension for which the core tension is equal to the total core capacity:

$$S\left(r,T_p(r)\right) = S_t\left(r,T_p(r)\right) \quad [15]$$

Combining [14] and [15] provides an expression that can be solved numerically to calculate the cable pullout tension:

$$T_p(r) = \frac{A_T}{A_S(r)}S_t\left(r,T_p(r)\right) \quad [16]$$

When the pullout tension is reached in the cable, the core is expected to pull out of the socket. The cable-socket assembly is therefore expected to fail when the cable pullout tension is reached for any core diameter.

3.6 Full Model

The variables and equations of the proposed mathematical model are summarized as follows:

Socket casting geometry R_0	Casting front radius [in]	
	β	Casting slope [rad]
	L_c	Casting length [in]
	L_w	Wire length in casting's longitudinal direction [in]
Core and Cable Variables r	Core radius [in]	
	T	Cable tension [kip]
Crossing wires geometry D_i	ith crossing wire diameter [in]	
	$\gamma_i(r)$	ith crossing wire angle with core surface [rad]
	$z_i(r)$	ith crossing wire crossing location [in]
Areas	A_T	Total wire area in cable section [in^2]
	$A_S(r)$	Total wire area in core section [in^2]
Material properties	c	Zinc cohesion [ksi]
	b	Wire-zinc bond strength [ksi]
	u	Wire nominal critical stress [ksi]
Friction coefficients	μ_{zz}	Zinc-zinc friction coefficient
	μ_{sz}	Socket-zinc friction coefficient
	μ_{wz}	Wire-zinc friction coefficient

Socket

Maximum pressure on socket surface:

$$p_0(T) = \frac{3T}{\pi L_c(3R_0 + L_c tan\beta)(tan\beta + \mu_{sz})}$$

Crossing wire

Nominal strength:

$$F_{ui}(r) = \frac{\pi {D_i}^2 u}{4}$$

Bond capacity with perimeter zinc:

$$F_{bi}(r) = \pi D_i b \frac{L_w - z_i(r)}{cos\gamma_i(r)}$$

Friction capacity with perimeter zinc:

$$F_{fi}(r,T) = \mu_{wz}\pi D_i p_0(T)(1 - 2\mu_{sz}tan\beta - tan^2\beta)\big(L_w - z_i(r)\big)\left(1 - \frac{L_w + z_i(r)}{2L_c}\right)$$

Maximum tension at crossing point:

$$F_i(r,\ T) = min\ \Big(F_{ui}(r),\ F_{bi}(r) + F_{fi}(r,T)\Big)$$

Core

Cohesion capacity $S_c(r) = 2\pi r L_c c$

Confinement friction capacity $S_{fc}(r,T) = \pi r \mu_{zz} L_c p_0(T)\ (1 - 2\mu_{sz} tan\beta - tan^2\beta)$

Crossing wires capacity: $S_w(r,T) = \sum_{i \in I(r)} F_i(r,T) cos\gamma_i(r)$

Crossing wires friction capacity: $S_{fw}(r,T) = \mu_{zz} \sum_{i \in I(r)} F_i(r,T)\ sin\gamma_i(r)$

Total capacity: $S_t(r,T) = S_c(r) + S_{fc}(r,T\ ) + S_w(r,T) + S_{fw}(r,T)$

Cable

Cable pullout tension: $T_p(r) = \frac{A_T}{A_S(r)} S_t\left(r, T_p(r)\right)$

4.0 Wire Brooms

The proposed model includes the contribution of the crossing wires to resist core pullout. To calculate this contribution, one must know which wires cross through the core surface and, for each crossing wire, the position of the crossing point and the angle between the wire and the socket axis at that point (Figure 13 above). These parameters depend on the core radius. In order to apply the proposed model to the sockets of interest, we extracted the wire broom geometry from laboratory observations. The wire broom is a description of the shape and position of each individual wire within the socket casting.

4.1 Method and Assumptions

For the six socket castings cut open in laboratories, we assembled the wire broom geometry as shown in Figure 17. The positions of the wire ends were measured on the transverse sections made at the back of each casting (Appendix M). For sockets M4-4_T, M8N_T, B4N_G and B12W_G, half of the casting was cut in the transverse direction for the wire broom study while the other half was used for other tests, such as mechanical testing of the zinc. In this case, the wire distribution was assumed to be symmetrical in the other half of the casting. At the front of the casting, the wires are assumed to remain tightly packed together up to socket's shoulder. Each wire position at the back of the socket was paired with a wire position at the front of the socket to obtain the wire broom. Each wire is assumed to be bent near the shoulder and to remain straight between the bend and the wire end. This is consistent with the wire shapes observed on the socket's longitudinal sections (section 2.1 above). This is also consistent with a cable socketing process where the wires are permanently (plastically) bent such that the wire broom remains open in the socket before casting the zinc.

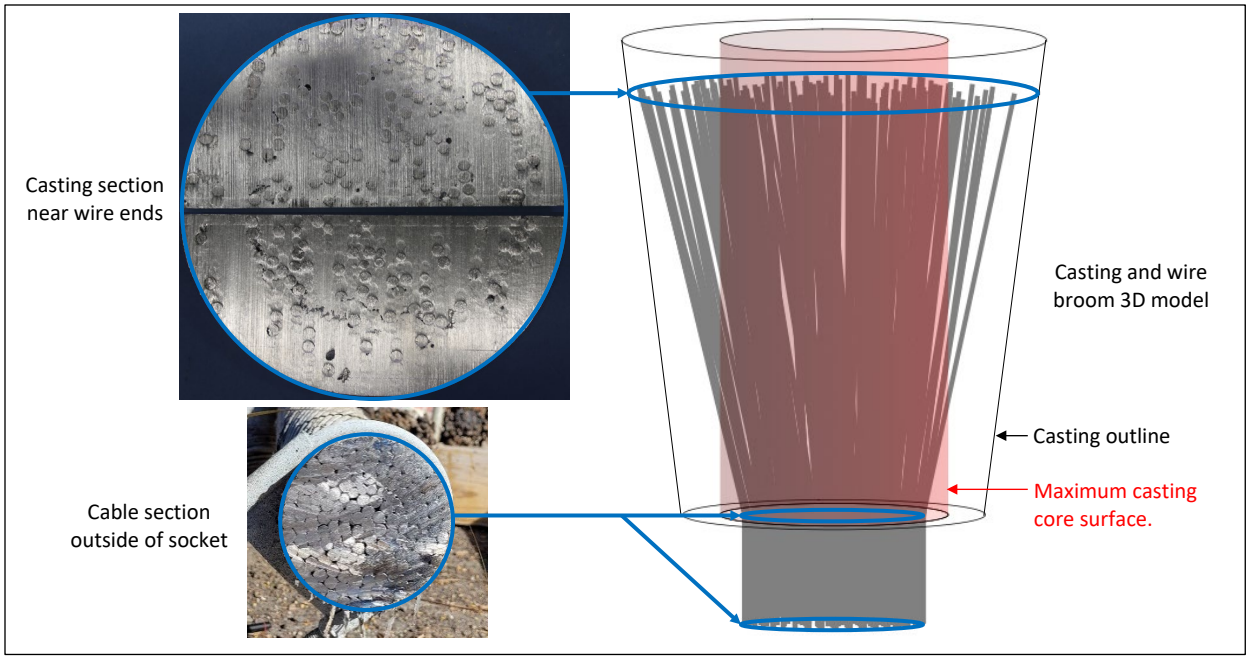

Figure 17: Broom geometry construction from cable and casting sections *(top photo: Socotec).*

4.2 Results

We assembled the wire broom geometry of the six sockets that were cut open in laboratories. These sockets are of three different types, corresponding to three different cable diameters. For each socket type, we also assembled a uniform wire broom where the wires ends are evenly spaced in the radial and circumferential directions. The uniform wire brooms are hypothetical and considered for comparison purpose only.

The actual and uniform wire brooms of auxiliary backstay ground-end sockets are shown in Figure 18. Socket B4S_G was tested to failure at Lehigh University, and socket B12W_G exhibited the largest cable slip across the entire telescope structure, with 1.875 inch. The broom of socket B12W_G is visually narrower than for the other sockets, with wires crossing the core surface closer to the wire ends, resulting on relatively short embedment lengths in the perimeter zinc.

The actual and uniform wire brooms of auxiliary main tower-end sockets are shown in Figure 19. Socket M4N_T is where the first cable failure occurred on August 10, 2020, and socket M8N_T exhibited a relatively small cable slip of 0.625 inch.

The actual and uniform wire brooms of original main tower-end sockets are shown in Figure 20. Socket M4-4_T is where the second cable failure occurred on November 6, 2020.

For each wire broom, the start and end position of every wire were saved in a database and used as input parameters when applying the proposed model to the telescope's sockets (section 5.0 below).

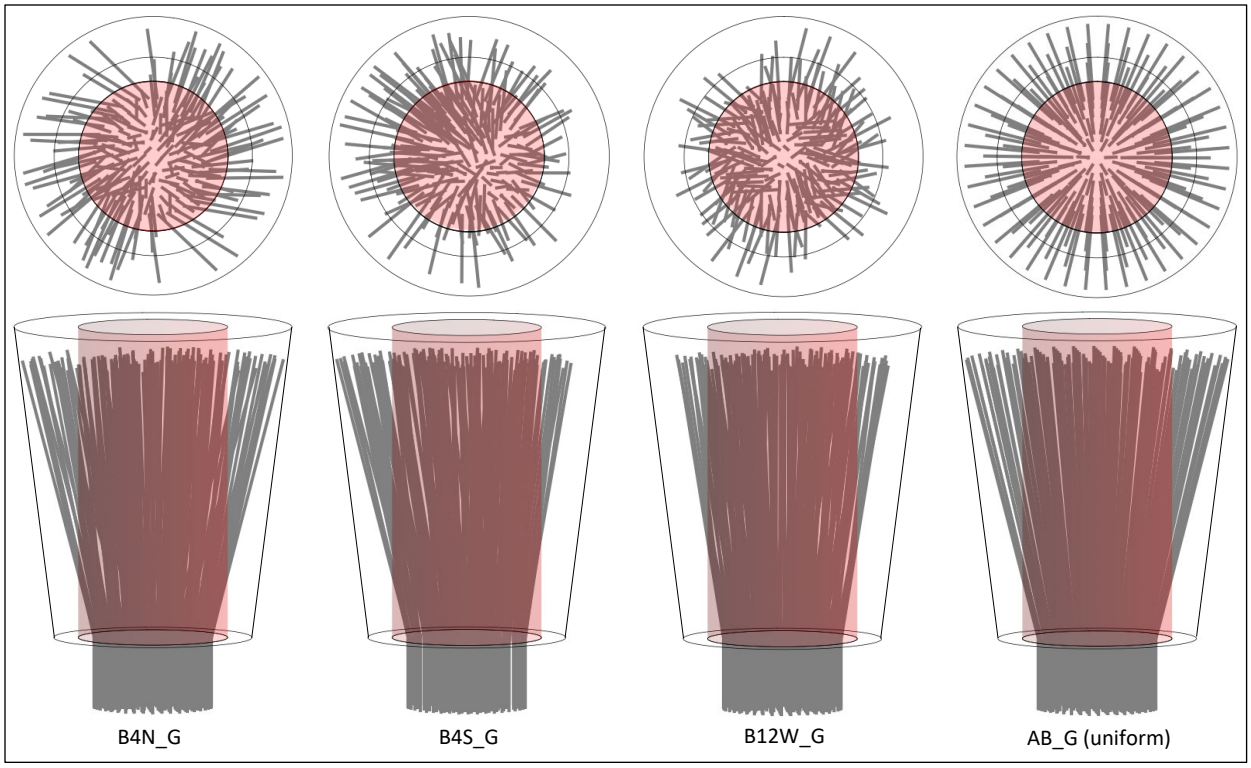

Figure 18: Auxiliary backstay ground-end socket brooms.
The maximum diameter core is highlighted in red.

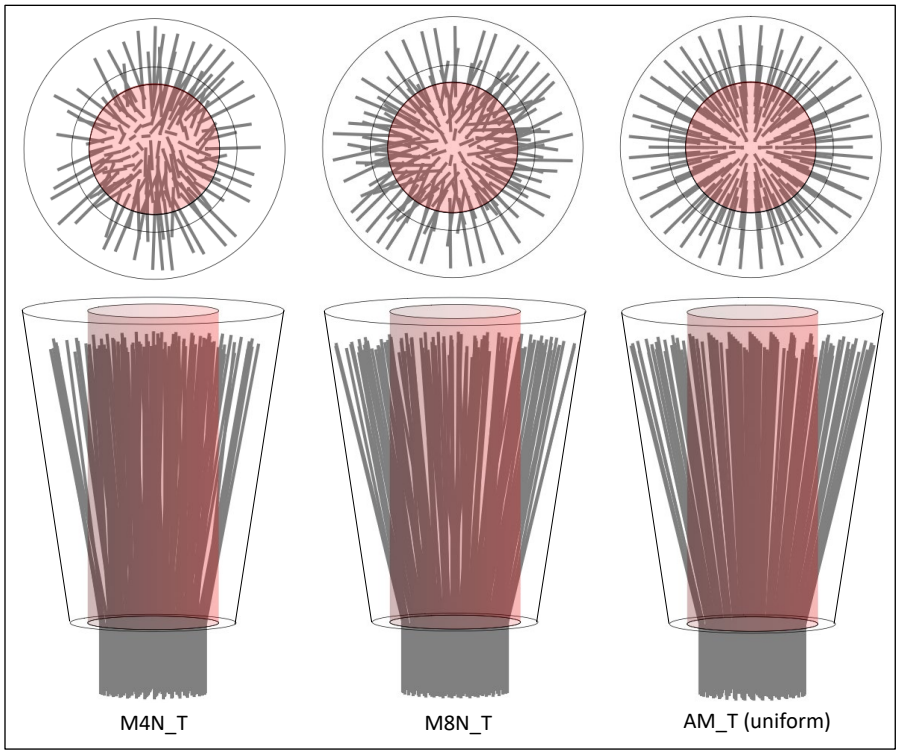

Figure 19: Auxiliary main tower-end socket brooms.
The maximum diameter core is highlighted in red.

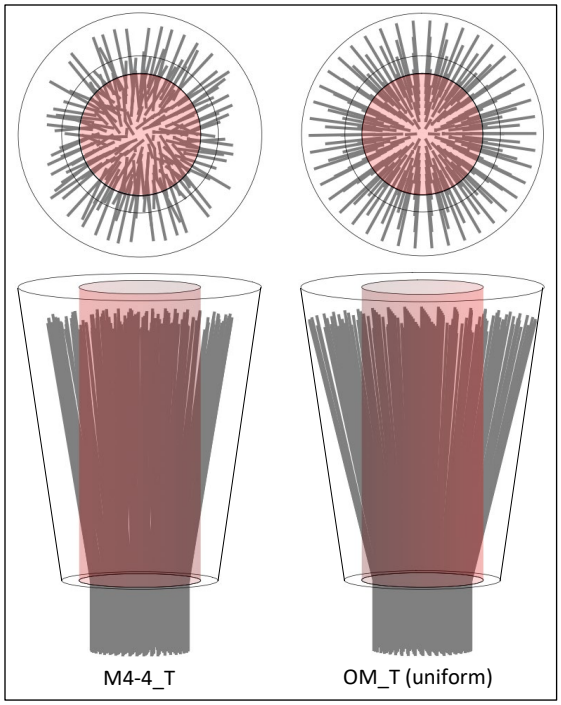

Figure 20: Original main tower-end socket brooms.

5.0 Model Application

5.1 Assumptions

The set of results presented below is based on the following material properties and friction coefficients:

- The wire nominal critical stress is taken as u = 202 kilopound per square inch (ksi). This is at mid-point between the yield stress of 169 ksi and the ultimate tensile stress of 227 ksi measured on average through testing of 12 wires of the telescope's cables (Appendix L).
- The zinc-to-zinc, socket-to-zinc and wire-to-zinc static friction coefficients are assumed to be 0.5. ($\mu_{zz} = \mu_{sz} = \mu_{wz} = 0.5$).
- The zinc's cohesion and the wire-to-zinc shear bond strength are assumed to be 1.02 ksi. ($b = c = 1.02$ ksi). This value was determined based on the results of the socket load test performed at Lehigh University (Appendix N), by equating the cable pullout tension predicted by the mathematical model with the actual failure load of 1,642 kip observed during the test. The wire-to-zinc shear bond strength was also measured experimentally by WJE-NESC as part of the investigation of the first socket failure[4], and the measured average strength was 1.07 ksi. This result is generally consistent with our cohesion and bond strength value derived from the socket load test.

[4] Wiss, Janney, Elstner Associates, *Arecibo Observatory - Auxiliary Main Cable Socket Failure Investigation*, 6/21/2021.

5.2 Results

5.2.1 Cable Pullout Tension and Critical Core

For a given core radius *r*, the cable pullout tension $T_p(r)$ is the tension in the entire cable when the core pulls out. The cable pullout tension is plotted in Figure 21 over a range of core radii for the six sockets of known wire broom geometry. The sockets are grouped by socket type and, for each socket type, a hypothetical socket with uniform wire broom is also included.

The cable pullout tension generally decreases as the core radius increases. A sharp drop in the cable pullout tension occurs each time the core radius increases past the radius of a wire layer at the front of the socket, where the wires are still tightly packed together in the cable section. As a new wire layer gets included in the enlarged core, the wire tension pulling on the core increases. For five of the six actual sockets, the cable pullout tension is minimum when the core radius is maximum. The only exception is socket M8N_T, but even in that case the minimum cable pullout tension is less than two percent lower than the cable pullout tension for the maximum core radius. This difference is negligible. To determine the minimum capacity of the cable pullout tension, we assume that the critical core is the largest possible core, whose radius is equal to the socket's front radius (i.e. $r = R_0$). The rest of results presented in this appendix are based on that assumption.

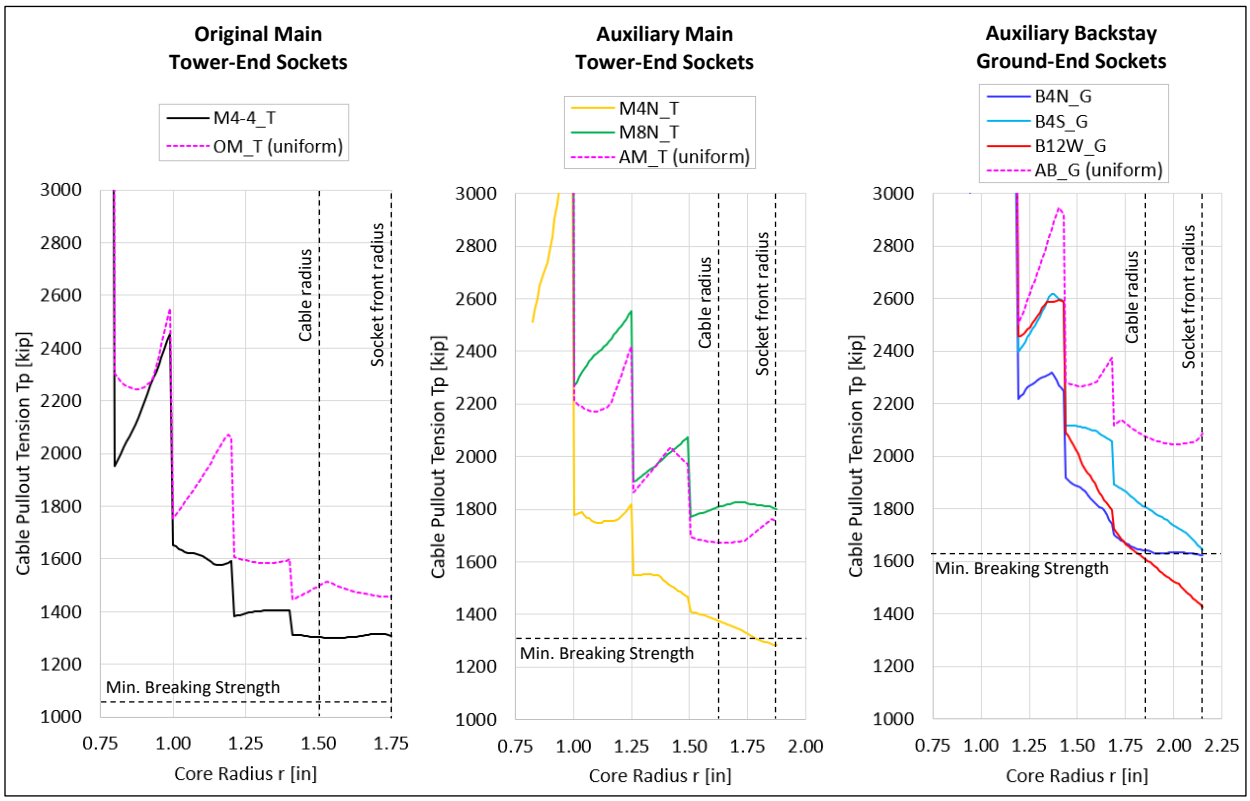

Figure 21: Cable pullout force vs core radius.

The cable pullout tension and Minimum Breaking Strength are compared in Table 1 for the sockets with uniform brooms. The pullout tension is 30 to 40 percent greater than the Minimum Breaking Strength, which is consistent with the expectation that a properly-installed spelter socket is stronger than the connected cable. Table 1 also compares the pullout tension and Minimum Breaking Strength for the same sockets in the hypothetical case where there is no wire broom, such that the cable tension can only be resisted by zinc cohesion and friction on the core

surface. In that case, the pullout tension is less than 15 percent of the Minimum Breaking Strength, which emphasizes the importance of the wire broom in spelter sockets.

The cable pullout tension and Minimum Breaking Strength are compared in Table 2 for the telescope's sockets, i.e. considering the actual wire brooms. The pullout tension is smaller than the Minimum Breaking Strength for sockets M4N_T and B12W_G. These are the two sockets where the maximum cable slips were measured prior to collapse. This result suggests a correlation between wire broom geometry and cable slip, which was further investigated.

Table 1: Cable Minimum Breaking Strength and pullout tension in sockets with uniform broom and no broom.

		OM_T Original Main Tower-end Socket	**AM_T** Auxiliary Main Tower-end Socket	**AB_G** Auxiliary Backstay Ground-end Socket
Cable Minimum Breaking Strength T_b [kip]		1,044	1,314	1,614
Uniform Broom	**Cable Pullout Tension $T_p = T_p(R_0)$ [kip]**	1,456	1,750	2,085
	Ratio T_p/T_b	1.39	1.33	1.29
No Broom	**Cable Pullout Tension $T_p = T_p(R_0)$ [kip]**	159	179	211
	Ratio T_p/T_b	0.15	0.14	0.13

Table 2: Cable Minimum Breaking Strength and pullout tension in actual sockets.

	M4-4_T	**M8N_T**	**B4S_G**	**B4N_G**	**M4N_T**	**B12W_G**
Cable Minimum Breaking Strength T_b [kip]	1,044	1,314	1,614	1,614	1,314	1,614
Cable Pullout Tension $T_p = T_p(R_0)$ [kip]	1,310	1,800	1,642	1,622	1,283	1,425
Ratio T_p/T_b	1.25	1.37	1.02	1.00	0.98	0.88
Cable Slip [in]	Unknown	0.625	0.875	0.875	1.125	1.875

5.2.2 Core Shear and Cable Slip

The large cable slips observed on some of the telescope's sockets are the result of two steps. First, the pre-stretching and/or initial loading of the cable caused the zinc casting to shift and deform to become tightly wedged into the socket. This is expected to occur in any zinc-filled spelter socket, and to result in a relatively small cable slip. Larger cable slips were observed in some of the sockets cut open in the laboratory. This increased slip was caused by the displacement of a core within the casting. This second step is the focus of our analysis.

For the core to displace within the casting, at least one of two mechanisms must occur. The first possible mechanism is a plastic deformation and/or creep of the zinc material near the core surface, which we refer to as *zinc flow*. Zinc flow is driven by a shear stress in the material in the flow direction. The second possible mechanism is the core slipping after the development of a fracture plane on the core surface. In that case, the core slips when a shear stress overcomes the bond and friction capacities on the core surface. Therefore, for either mechanism, the casting core can only displace if there is a shear stress acting on the core surface. Conversely, the core cannot displace when the full cable tension is resisted by the crossing wires, such that there is no shear stress on the core surface. The shear stress on the core surface is simply referred to *core shear* in the following.

We performed an analysis to evaluate the core shear in the telescope's sockets. When a socket is initially loaded, the cable tension is resisted by a combination of core shear and crossing wire tension. The split between those two resisting forces depends on the relative stiffnesses of the zinc and wires, which is not considered in the socket strength model developed above. However, the model can be used to determine the minimum core shear needed to resist a cable tension. For a given cable tension T, and considering the maximum core radius R_0, the crossing wires capacity S_w is calculated first:

$$S_w = S_w(R_0, T)$$

The surface area of the core is as follows:

$$A_c = 2\pi R_0 L_c$$

If the crossing wires capacity S_w is less than the cable tension T, the difference must be resisted as core shear. We note τ_c the minimum core shear needed to resist the cable tension T:

$$\tau_c = max\left(\frac{T - S_w}{A_c}, 0\right)$$

The maximum cable tension that can be resisted without any core shear can also be calculated. Noted T_{ns}, it is calculated by solving the following equation numerically:

$$T_{ns} = S_w(R_0, T_{ns})$$

Results are provided in Table 3 for the sockets with uniform broom. When the cable safety factor is two, which is the approximate safety factor in the telescope's cables, no core shear is needed in any of the three sockets. The minimum safety factor to not need core shear ranges from 1.5 to 1.9.

Results are provided in Table 4 for the telescope's sockets, i.e. considering the actual wire brooms. The core shear needed was calculated for two loading conditions: gravity loads only, which the telescope experienced for most of its lifetime, and hurricane Maria as representative of an extreme event. The cable tensions for both conditions were determined through analysis (Appendix G and Appendix J). For the five auxiliary sockets, the cable slip increases with the core shear needed under gravity loads. This correlation is plotted in Figure 22. The hurricane condition can cause a significant increase in core shear needed, such that cable slip may have been activated or accelerated during significant windstorms. Socket M4-4_T experienced a 20 percent load increase when the first cable failed, and per our model this event increased the core shear needed from zero to the highest value among the sockets considered (0.70 ksi). The minimum safety factor to not need core shear ranges from 1.7 to 3.0, and those minimum and maximum values are for the sockets exhibiting the minimum and maximum cable slips, respectively.

Table 3: Core shear analysis results in sockets with uniform broom.

	OM_T **Original Main Tower-end Socket**	**AM_T** **Auxiliary Main Tower-end Socket**	**AB_G** **Auxiliary Backstay Ground-end Socket**
Cable Minimum Breaking Strength T_b [kip]	1,044	1,314	1,614
Cable Tension T = T_b/2.0[(1)] [kip]	522	657	807
Crossing Wires Capacity S_w [kip]	648	753	862
Core Shear Needed τ_c [ksi]	0	0	0
Cable Safety Factor T_b/T	2.0	2.0	2.0
Max. Cable Tension to Not Need Core Shear T_{ns} [kip]	674	763	869
Min. Cable Safety Factor to Not Need Core Shear T_b/T_{ns}	1.5	1.7	1.9

(1) 2.0 is the assumed cable safety factor.

Table 4: Core shear analysis results needed in telescope sockets.

		Before M4N Failure						After M4N Failure
		M4-4_T	M8N_T	B4S_G	B4N_G	M4N_T	B12W_G	M4-4_T
Cable Slip [in]		Unknown	0.625	0.875	0.875	1.125	1.875	Observed
Core Surface Area Ac [in²]		93	106	122	122	106	122	93
Cable Minimum Breaking Strength T_b [kip]		1,044	1,314	1,614	1,614	1,314	1,614	1,044
Under Gravity Loads	**Cable Tension T [kip]**	534	602	665	698	600	624	646
	Crossing Wires Capacity S_w [kip]	565	752	659	671	554	561	581
	Core Shear Needed τ_c [ksi]	0	0	0.05	0.22	0.43	0.52	0.70
	Cable Safety Factor T_b/T	2.0	2.2	2.4	2.3	2.2	2.6	1.6
Maximum During Hurricane Maria	**Cable Tension T [kip]**	543	636	687	721	631	647	-
	Crossing Wires Capacity S_w [kip]	567	761	662	674	558	565	-
	Core Shear Needed τ_c [ksi]	0	0	0.20	0.39	0.69	0.67	-
	Shear Stress Increase vs. Gravity	-	-	+283%	+73%	+58%	+29%	-
	Cable Safety Factor T_b/T	1.9	2.1	2.3	2.2	2.1	2.5	-
Max. Cable Tension to Not Need Core Shear T_{ns} [kip]		571	796	657	666	547	540	571
Min. Cable Safety Factor to Not Need Core Shear T_b/T_{ns}		1.8	1.7	2.5	2.4	2.4	3.0	1.8

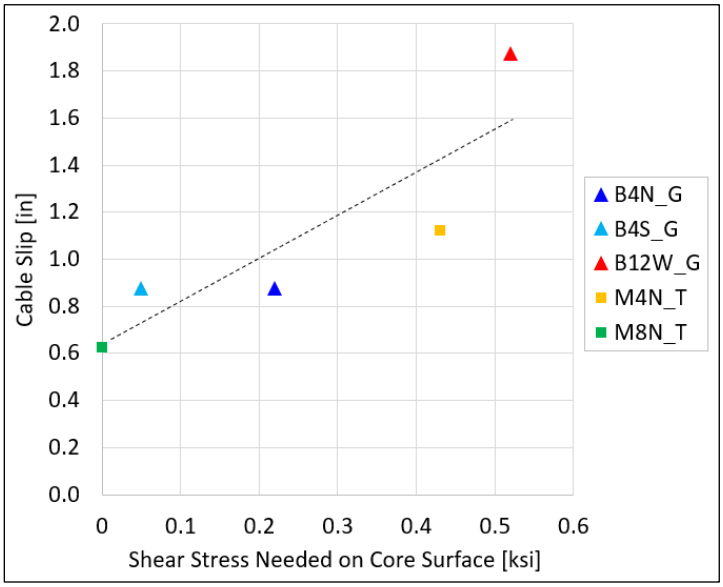

Figure 22: Cable slip vs. core shear needed in auxiliary sockets under gravity loads before M4N failure.

The above results are consistent with the socket behavior shown in Figure 23 and Figure 24, where the zinc material flows as long as it is subjected to shear stress. When the socket is initially loaded, the cable tension is partially resisted by core shear, which causes zinc flow. As zinc flows, the casting core displaces and the crossing wires stretch, causing an increase in crossing wire tension and therefore a decrease in core shear. If the crossing wires can resist the full cable tension (Figure 23), the core shear eventually drops to zero and zinc flow stops. But if the crossing wires cannot resist the full cable tension (Figure 24), zinc flows continues and leads to the large cable slips and eventual socket failures observed on the telescope.

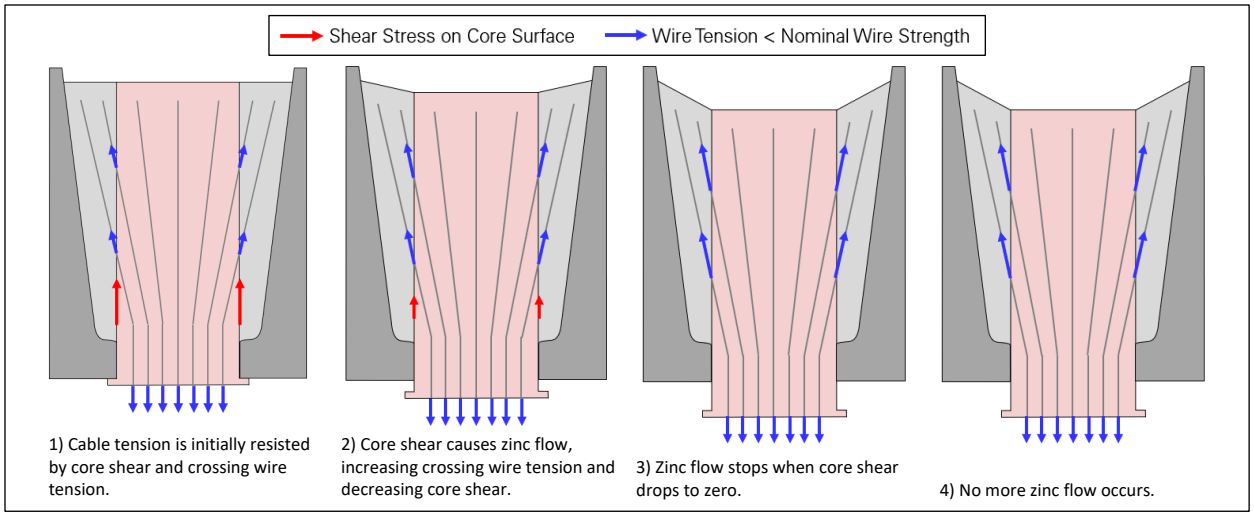

Figure 23: Limited cable slip in socket with crossing wire capacity sufficient to resist full cable tension.

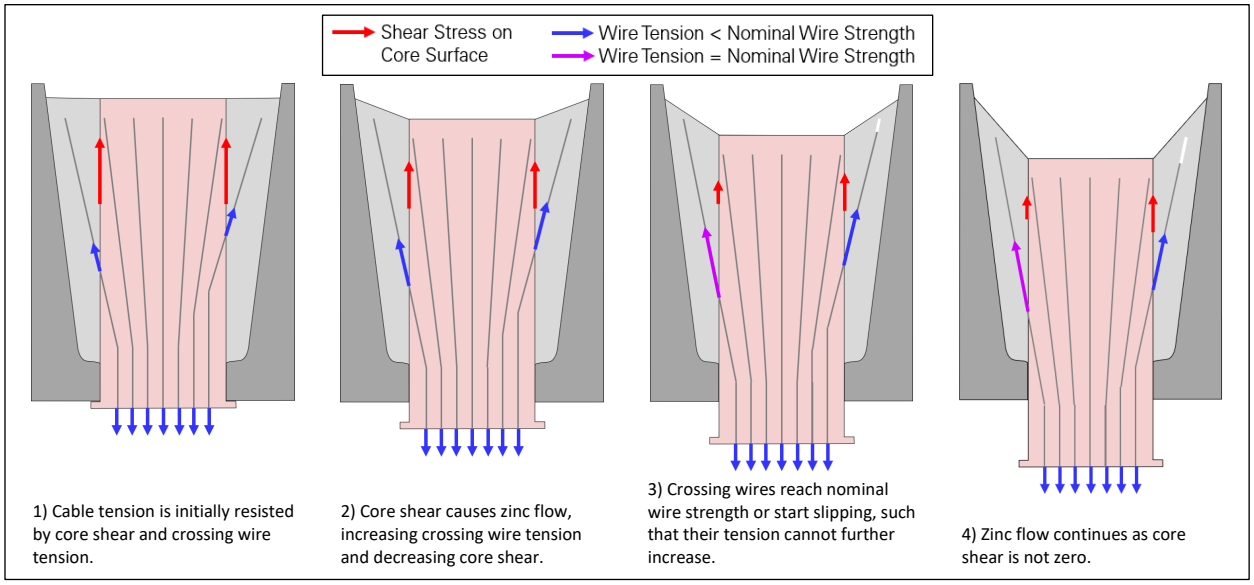

Figure 24: Continued zinc flow and cable slip in socket with crossing wire capacity insufficient to resist full cable tension.

5.2.3 Socket Failure Mode

Two general failure modes were observed on the telescope's sockets : *core rupture*, and *core flow-out*.

The failures of sockets M4N_T and M4-4_T in the field involved the rupture of multiple outer wires inside the socket and a significant displacement or complete pull-out of the casting core. We refer to this failure mode as *core rupture*. The load test of socket B4S_G was stopped after seven outer wires ruptured inside the socket, and the cable slip measurements and post-test laboratory analysis revealed that the casting core had displaced significantly. Socket B4S_G was therefore on the brink of experiencing core rupture like M4N_T and M4-4_T. Core rupture occurred when the cable slip was 1.125 inch and 1.375 inch in M4N_T and B4S_G, respectively. Cable slip could not be measured in M4-4_T as the socket's front was not visible at the top of Tower 4.

Socket B12W_G exhibited the largest cable slip among the telescope's sockets, with 1.875 inch. However, the socket did not fail or experience any wire rupture. The laboratory analysis revealed that in B12W_G, the crossing wire ends slipped with respect to the zinc outside of the core and moved towards the front of the socket in parallel with the core. It is evident that if the displacement of the core and crossing wires had continued, the socket would eventually have failed due to reduced contact area between cable and socket and/or extreme strain of the wires and zinc materials. This failure mode is referred to as *core flow-out*.

From the laboratory observations, it appears that B12W_G experienced core flow-out instead of core rupture due to its crossing wires' tendency to slip instead of rupturing. To test this hypothesis, we compared the number of fully developed wires (rupture before slipping) and partially developed wires (slip before rupturing) in the sockets analyzed. We define a socket's *wire development ratio* as the fraction of crossing wires that are fully developed. The wire development ratio is therefore a measure of the general tendency for the crossing wires to slip (low ratio) or rupture (high ratio) in a given socket. The wire development ratio depends on the cable tension, as a higher tension causes in a higher radial compressive stress in the socket, allowing to develop more friction between wires and zinc to resist wire slip.

Results are provided in Table 5 for the sockets with uniform wire brooms, assuming a cable tension equal to half of the cable's Minimum Breaking Strength. The wire development ratios range between 59 and 73 percent, such that a majority of the crossing wires would rupture before slipping in those sockets. However, since the crossing wires could have resisted the full cable tension (Table 3 page 21) zinc flow would have stopped, and the crossing wires would not have rupture nor slipped.

Results are provided in Table 6 for the telescope's sockets, i.e. considering the actual wire brooms. The wire development ratio was determined under gravity loads and, when applicable, for the failure load. Among the failed and failing sockets, the three sockets experiencing core rupture have a higher wire development ratio (59 to 66 percent) than the socket experiencing core flow-out (38 percent). The fully and partially developed crossing wires are shown in Figure 25 for those four sockets.

Table 5: Crossing wire development analysis results in sockets with uniform broom.

	OM_T Original Main Tower-end Socket	**AM_T** Auxiliary Main Tower-end Socket	**AB_G** Auxiliary Backstay Tower-end Socket
Cable Minimum Breaking Strength T_b [kip]	1,044	1,314	1,614
Cable Tension T/2.0 [kip]	522	657	807
Cable Safety Factor T_b/T	2.0	2.0	2.0
Number of Wires N	168	126	164
Number of Crossing Wires N_c	132	90	102
Number of Fully Developed Crossing Wires N_{cf}	78	66	74
Wire Development Ratio N_{cf}/N_c	59%	73%	73%

Table 6: Crossing wire development analysis results in telescope sockets.

	Gravity Loads Before M4N Failure						Gravity Loads After M4N Failure	End of Load Test
	M4-4_T	**M8N_T**	**B4S_G**	**B4N_G**	**M4N_T**	**B12W_G**	**M4-4_T**	**B4S_G**
Cable Slip [in]	Unknown	0.625	0.875	0.875	1.125	1.875	Observed	1.375
Number of Wires N	168	126	164	164	126	164	168	164
Number of Crossing Wires N_c	110	102	97	86	71	84	110	97
Number of Fully Developed Crossing Wires N_{cf}	64	44	46	52	42	32	72	64
Wire Development Ratio N_{cf}/N_c	58%	43%	47%	60%	59%	38%	65%	66%
Socket Failure Mode	None	None	None	None	Core Rupture	Core Flow-out	Core Rupture	Core Rupture

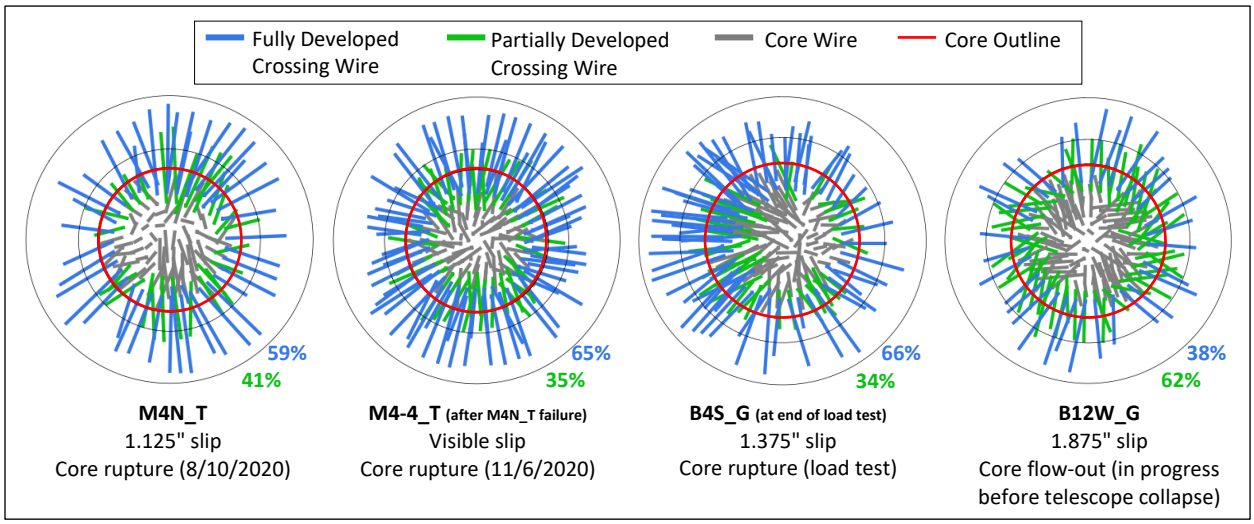

Figure 25: Fully and partially developed crossing wires in failed and failing sockets.

The above results are consistent with the socket behavior idealized in Figure 26 and Figure 27. In both cases, the crossing wires cannot resist the full cable tension, such that zinc flow cannot stop and the socket is bound to fail. The failure mode, however, depends on whether the crossing wires are fully or partially developed. If the crossing wires are fully developed (Figure 26), they continue to stretch near the core surface as the zinc continues to flow. Some of the wires rupture when they reach their ultimate tensile strain, which increases core shear and accelerates zinc flow, leading to more wire ruptures and, eventually, to core rupture. If the crossing wires are partially developed (Figure 27), they can slip in parallel with the cable instead of rupturing. In this case, the cable continues to gradually slip out of the socket. Complete slip-out or rupture will eventually occur as the contact length between cable and socket decreases and/or the zinc's strain becomes too large. Macroscopically, the socket failure is more brittle when the crossing wires are fully developed, and more ductile when the crossing wires are partially developed. Actual sockets include both fully and partially developed crossing wires and can therefore exhibit intermediate behaviors and failure modes.

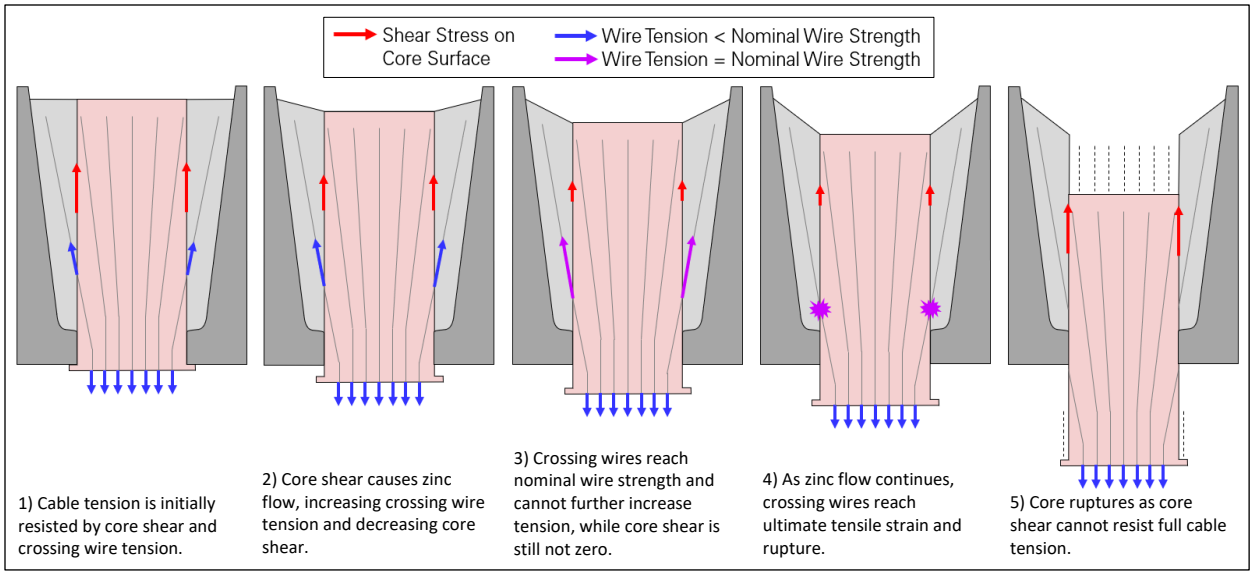

Figure 26: Core rupture in socket where crossing wires cannot resist full cable tension and are fully developed.

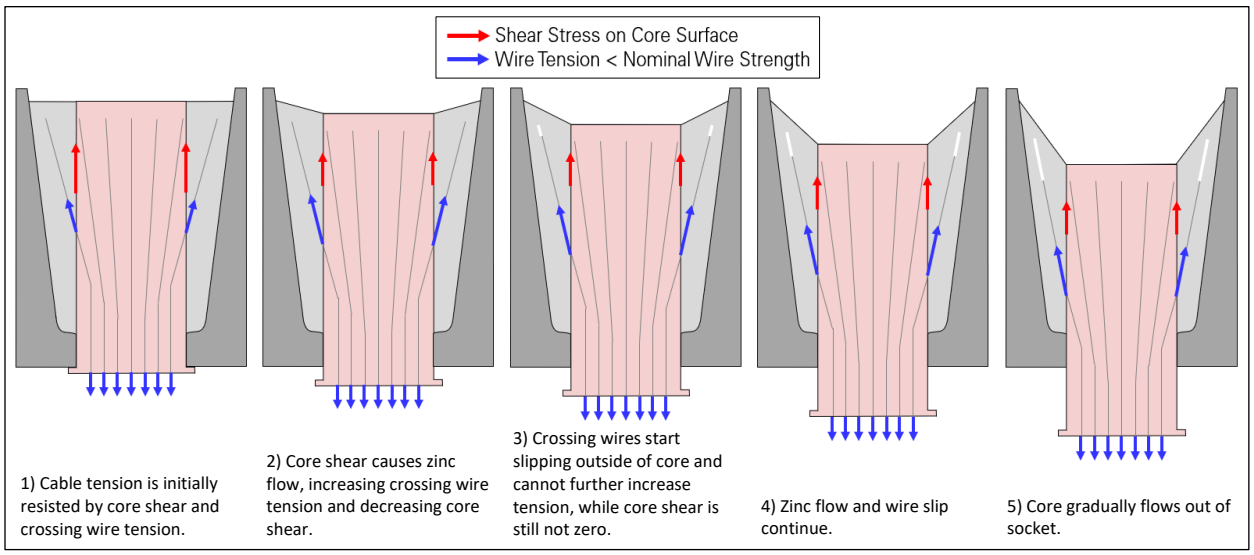

Figure 27: Core flow-out in socket where crossing wires cannot resist full cable tension and are partially developed.

5.2.4 Summary

By applying the proposed mathematical model to the six telescope sockets of known wire broom, we observed correlations between core shear, wire development ratio, cable slip and socket failure mode. These correlations are summarized in Figure 28 for the auxiliary sockets. The original socket (M4-4_T) is not included because its cable slip is not known. The left side of Figure 28 shows that the cable slip observed in the field increases with the core shear needed to resist the cable tension under gravity loads (same as Figure 22 page 22). This core shear depends on the collective capacity of the crossing wires to resist the cable tension: if the crossing wires capacity is lower, the core shear needed is higher. The right side of Figure 28 shows that failure occurs in the sockets exhibiting the largest cable slips, with a failure mode that depends on the wire development ratio: the socket experiences core rupture if its crossing wires tend to rupture before slipping (high ratio), and core flow-out if its wires tend to slip

before rupturing (low ratio). Both the cable slip and the socket failure mode are affected by the wire broom geometry, which is therefore key to the strength of a zinc-filled spelter socket. A summary of the cable safety factors, core shear needed, cable slip, wire development ratio and socket failure modes is provided in Table 7.

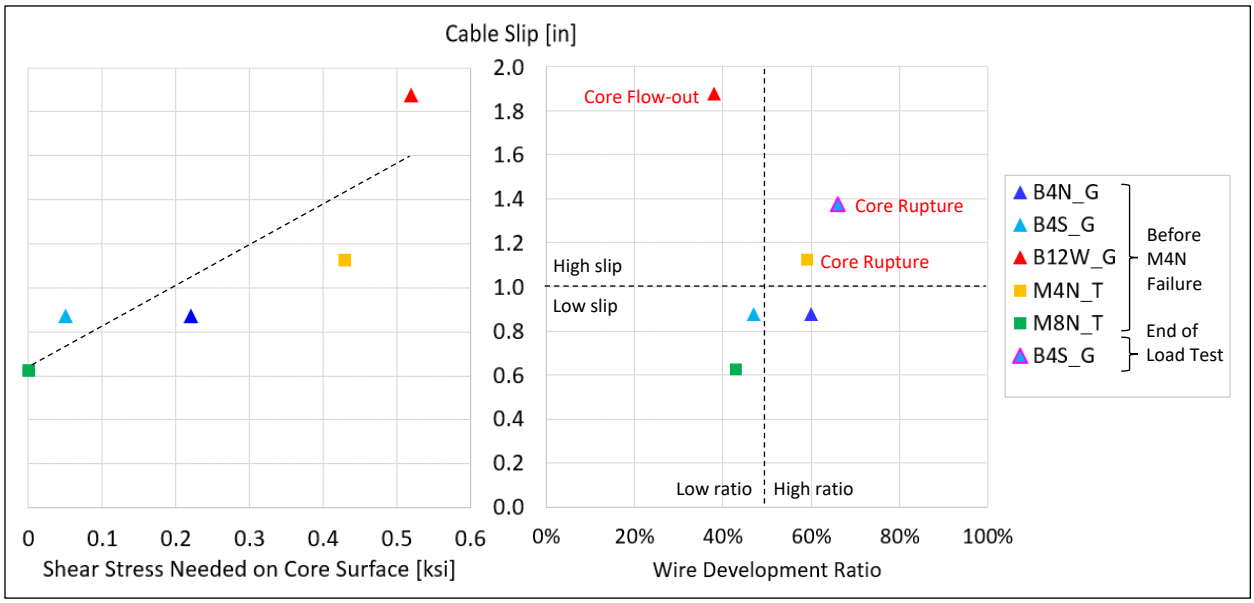

Figure 28: Correlation between core shear, wire development ratio, cable slip, and socket failure.

Table 7: Core shear, wire development ratio, cable slip, and socket failure mode.

	Under Gravity Before M4N Failure						Under Gravity After M4N Failure	At End of Load Test
	M4-4_T	**M8N_T**	**B4S_G**	**B4N_G**	**M4N_T**	**B12W_G**	**M4-4_T**	**B4S_G**
Min. Cable Safety Factor to Not Need Core Shear	1.8	1.7	2.5	2.4	2.4	3.0	1.8	2.5
Actual Cable Safety Factor	2.0	2.2	2.4	2.3	2.2	2.6	1.6	0.98
Core Shear Needed [ksi]	0	0	0.05	0.22	0.43	0.52	0.70	7.26
Cable Slip [in]	Unknown	0.625	0.875	0.875	1.125	1.875	Observed	1.375
Wire Development Ratio	58%	43%	47%	60%	59%	38%	65%	66%
Socket Failure Mode	None	None	None	None	Core Rupture	Core Flow-out	Core Rupture	Core Rupture

5.2.5 Illustration

Based on the above analysis results, the behavior of the six telescope sockets considered is described in the following through the lens of the proposed socket strength model (Figure 29 through Figure 34). It is understood that the proposed model simplifies and approximates the socket behavior.

Socket M4-4_T

1. As the socket is initially loaded, the cable tension is resisted by a combination of core shear and crossing wire tension.
2. Core shear causes zinc flow, which increases crossing wire tension and decreases core shear. The crossing wires capacity (565 kip) is greater than the cable tension (534 kip), so the core shear eventually drops to zero and zinc flow stops.
3. The first cable failure (M4N) on August 10, 2020 causes a 20 percent increase in cable tension, which reactivates zinc flow.
4. The new crossing wires capacity (581 kip) is less than the new cable tension (646 kip), so core shear (0.70 ksi) is still needed to resist the cable tension after the crossing wires reach their capacity. Most of the crossing wires (65 percent) are fully developed and reach their nominal strength.
5. As zinc flow continues, the fully developed crossing wires reach their ultimate tensile strain and rupture.
6. The core ruptures as core shear cannot resist the full cable tension, but the remaining wires rupture before the core fully slips out.

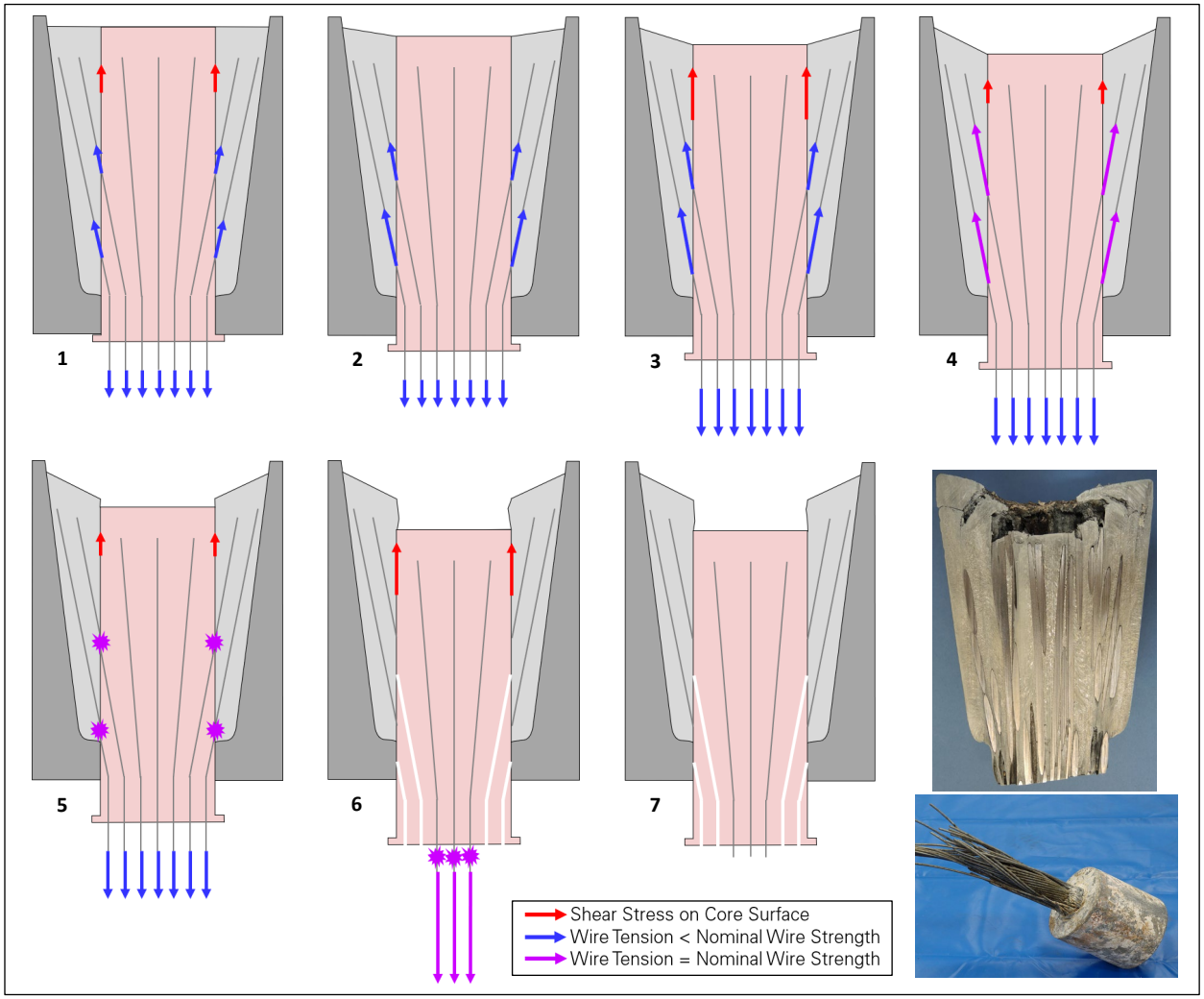

Figure 29: Behavior and failure of socket M4-4_T *(photos: Socotec).*

Socket M8N_T

1. As the socket is initially loaded, the cable tension is resisted by a combination of core shear and crossing wire tension.
2. Core shear causes zinc flow, which increases crossing wire tension and decreases core shear. The crossing wires capacity (752 kip) is greater than the cable tension (602 kip), so the core shear eventually drops to zero and zinc flow stops.

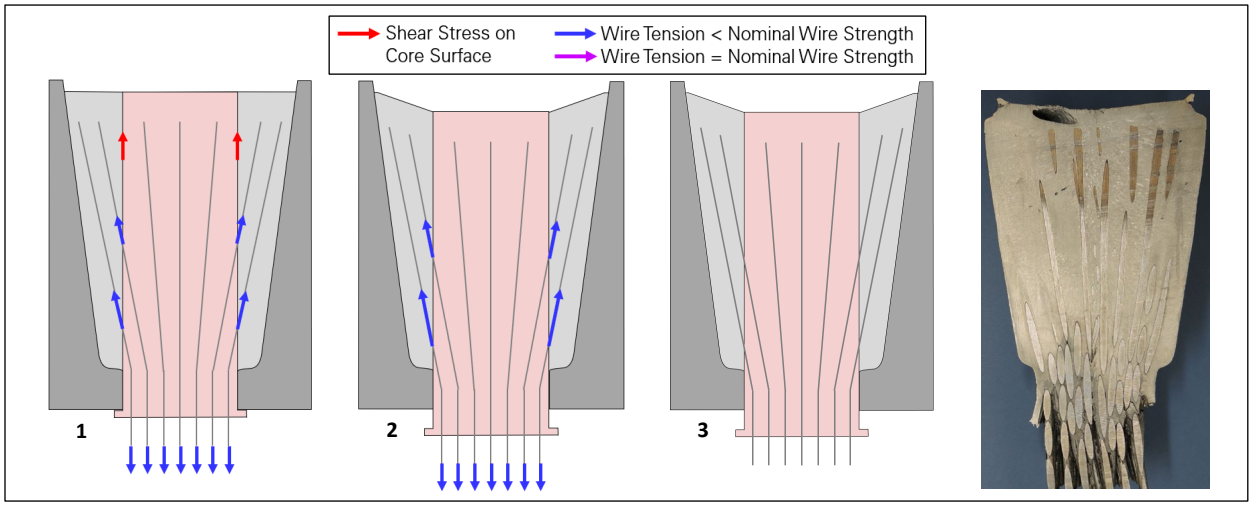

Figure 30: Behavior of socket M8N_T *(photo: Socotec).*

Socket B4N_G

1. As the socket is initially loaded, the cable tension is resisted by a combination of core shear and crossing wire tension.
2. Core shear causes zinc flow, which increases crossing wire tension and decreases core shear. The crossing wires capacity (671 kip) is less than the cable tension (698 kip), so core shear (0.22 ksi) is still needed to resist the cable tension after the crossing wires reach their capacity.
3. The core shear needed is relatively low, so zinc flow is slow, and the socket does not fail before the telescope's collapse.

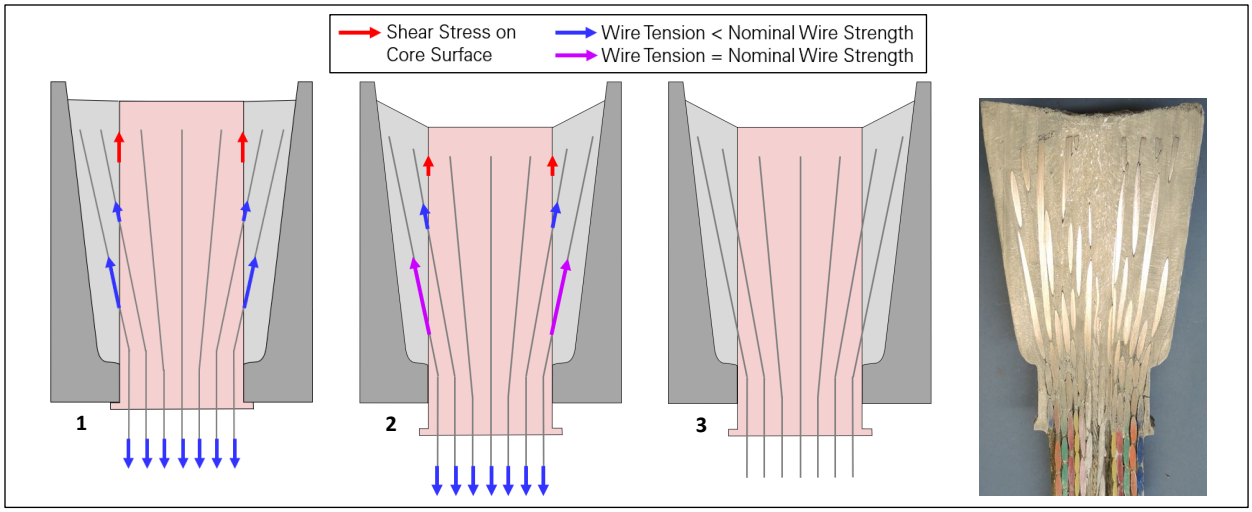

Figure 31: Behavior of socket B4N_G *(photo: Socotec).*

Socket B4S_G

1. As the socket is initially loaded, the cable tension is resisted by a combination of core shear and crossing wire tension.
2. Core shear causes zinc flow, which increases crossing wire tension and decreases core shear. The crossing wires capacity (659 kip) is less than the cable tension (665 kip), so core shear (0.05 ksi) is still needed to resist the cable tension after the crossing wires reach their capacity.
3. The core shear needed is relatively low, so zinc flow is slow, and the socket does not fail before the telescope's collapse.
4. As the socket is load-tested after the collapse, the maximum cable tension reached (1,647 kip) is higher than the cable's Minimum Breaking Strength (1,614 kip), and much higher than the crossing wires capacity. This activates a fast zinc flow and/or core fracture. Most of the crossing wires (66 percent) are fully developed and reach their nominal strength.
5. As zinc flow and/or core fracture continues to develop, some of the fully developed crossing wires rupture.
6. The test is ended by dropping the cable tension before the socket fails completely.

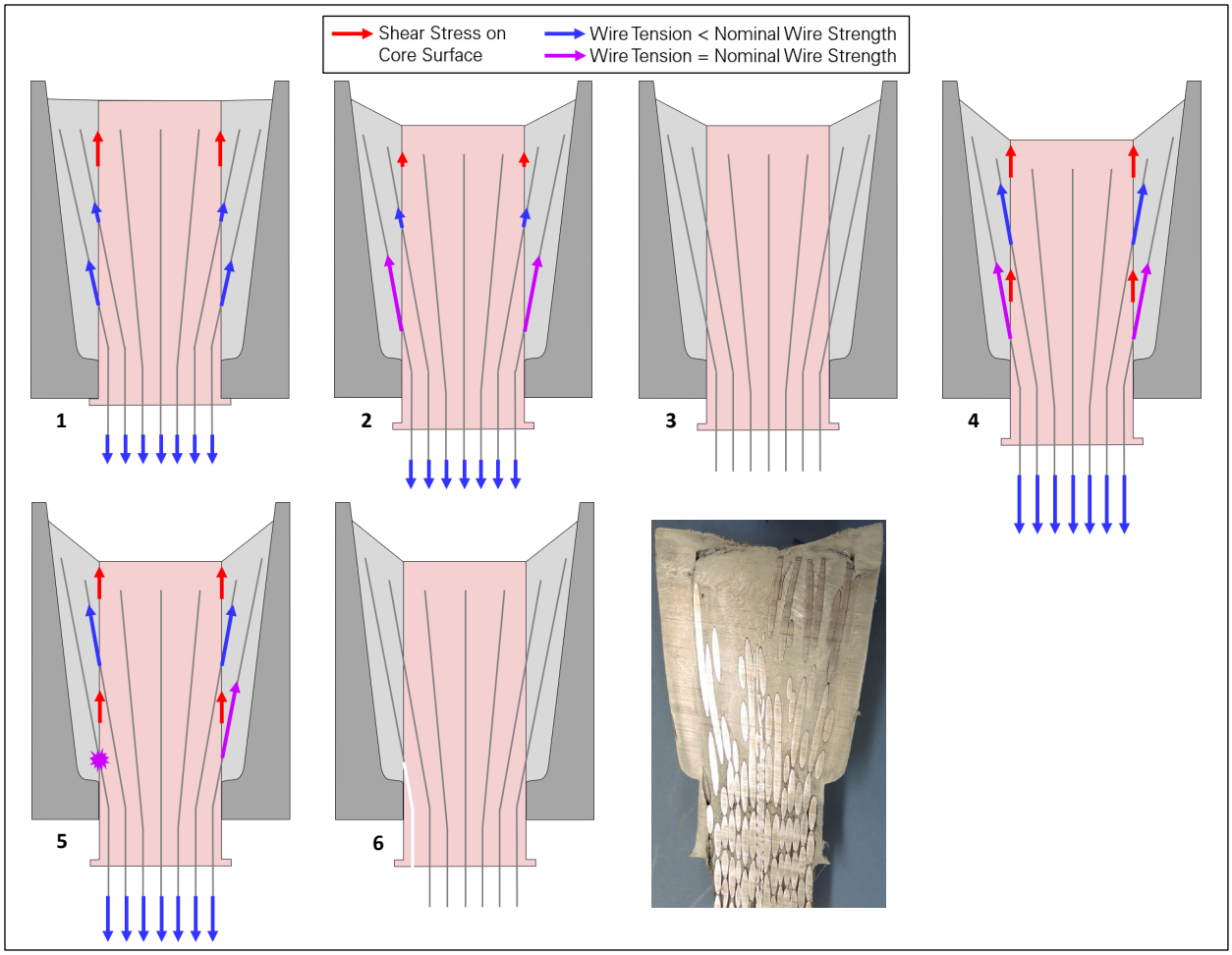

Figure 32: Behavior and failure of socket B4S_G *(photo: Socotec).*

Socket M4N_T

1. As the socket is initially loaded, the cable tension is resisted by a combination of core shear and crossing wire tension.
2. Core shear causes zinc flow, which increases crossing wire tension and decreases core shear. The crossing wires capacity (554 kip) is less than the cable tension (600 kip), so core shear (0.43 ksi) is still needed to resist the cable tension after the crossing wires reach their capacity. Most of the crossing wires (59 percent) are fully developed and reach their nominal strength.
3. As zinc flow continues, the fully developed crossing wires reach their ultimate tensile strain and rupture.
4. The core ruptures and slips out of the socket as core shear cannot resist the full cable tension.

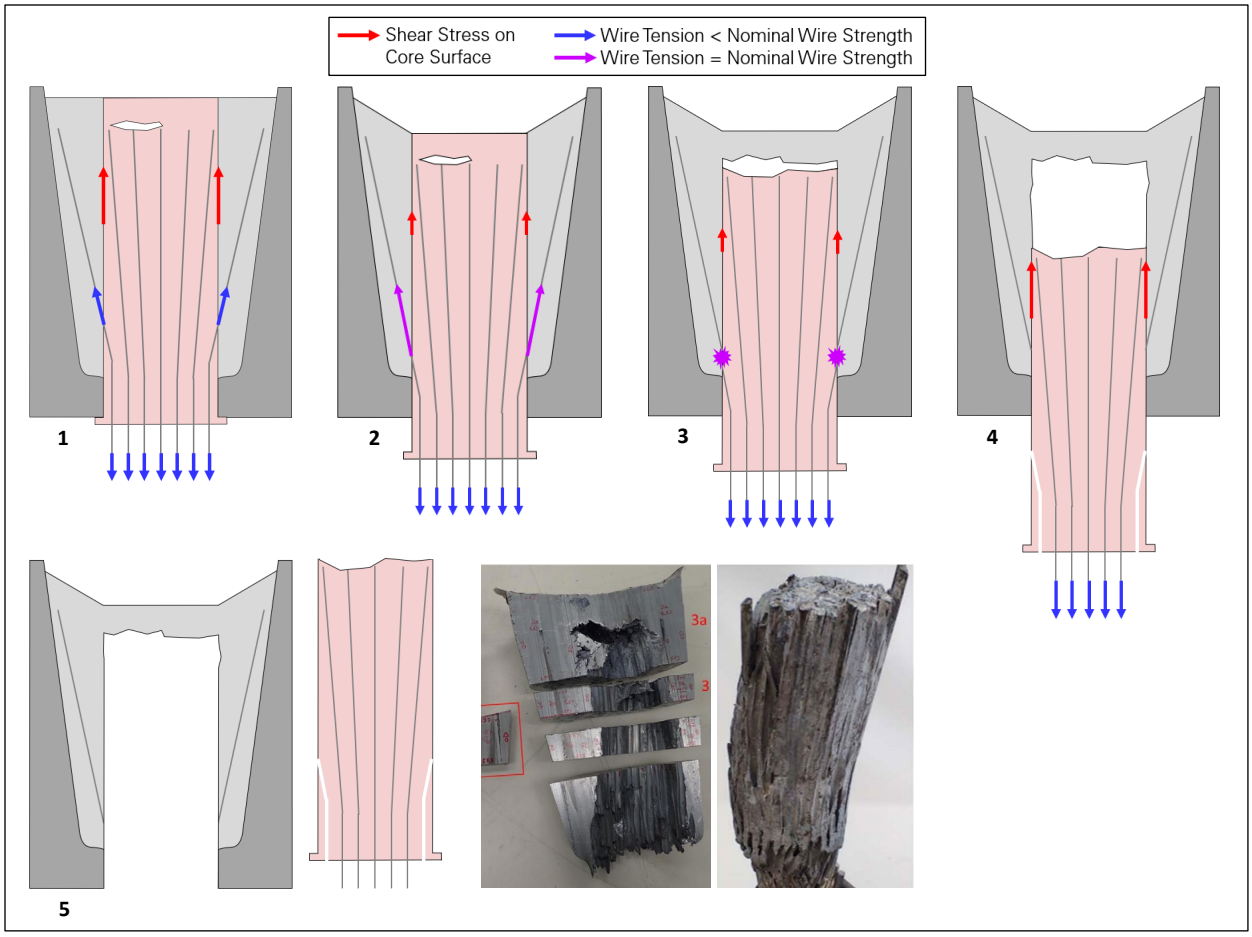

Figure 33: Behavior and failure of socket M4N_T *(photos: WJE[5]).*

[5] Wiss, Janney, Elstner Associates (WJE). *Auxiliary Main Cable Socket Failure Investigation.* June 21, 2021. Draft report provided by WJE.

Socket B12W_G

1. As the socket is initially loaded, the cable tension is resisted by a combination of core shear and crossing wire tension.
2. Core shear causes zinc flow, which increases crossing wire tension and decreases core shear. The crossing wires capacity (561 kip) is less than the cable tension (624 kip), so core shear (0.52 ksi) is still needed to resist the cable tension after the crossing wires reach their capacity. Most of the crossing wires (62 percent) are partially developed and start slipping before reaching their nominal strength.
3. As zinc flow continues, the partially developed crossing wires continue to slip as the core gradually flows out of the socket. This delays the socket failure, which does not occur before the telescope's collapse.

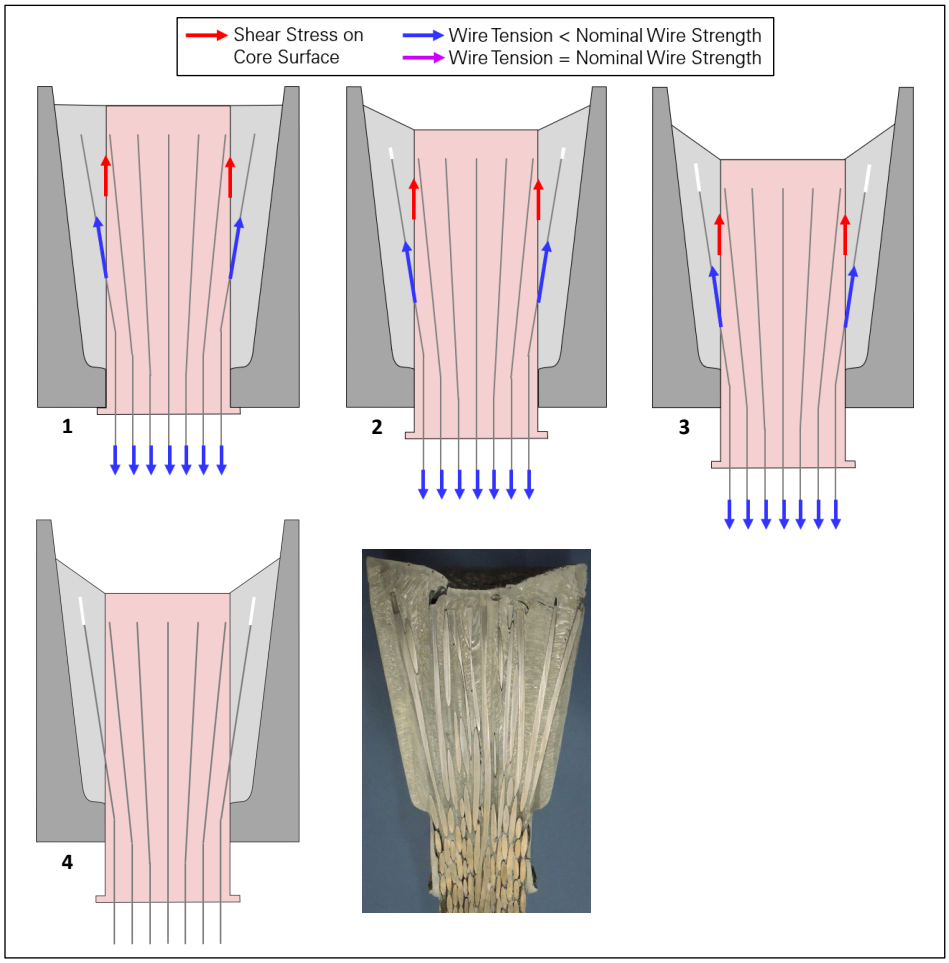

Figure 34: Behavior of socket B12W_G *(photo: Socotec).*